Elevated CO_2 alters soybean physiology and defense responses, and has disparate effects on susceptibility to diverse microbial pathogens

Melissa Bredow[1#], Ekkachai Khwanbua[1#], Aline Sartor Chicowski[1#], Matthew W. Breitzman[2], Yunhui Qi[3], Katerina L. Holan[1,4], Peng Liu[3], Michelle A. Graham[4] and Steven A. Whitham[1*]

[1] Department of Plant Pathology, Entomology & Microbiology, Iowa State University, Ames, IA 50011, USA

[2] W. M. Keck Metabolomics Research Laboratory, Iowa State University, Ames, IA 50011, USA

[3] Department of Statistics, Iowa State University, Ames, IA 50011, USA

[4] United States Department of Agriculture (USDA), Agricultural Research Service (ARS), Corn Insects and Crop Genetics Research Unit and Department of Agronomy, Iowa State University, Ames, IA 50011, USA

[#]Authors contributed equally to this work.
*Corresponding author: Steven Whitham (swhitham@iastate.edu)

ORCIDs:

Melissa Bredow	0000-0002-5564-9646
Ekkachai Khwanbua	0009-0007-4013-941X
Aline Sartor Chicowski	0000-0002-0949-2617
Matthew W. Breitzman	0000-0001-8673-1530
Yunhui Qi	0009-0009-6876-8888
Katerina L. Holan	0000-0002-3136-0805
Peng Liu	0000-0002-2093-8018
Michelle A. Graham	0000-0002-9842-7701
Steven A. Whitham	0000-0003-3542-3188

Keywords: *Glycine max*, carbon dioxide, plant immunity, *Pseudomonas syringae*, soybean mosaic virus, bean pod mottle virus, *Fusarium virguliforme*, *Pythium sylvaticum*, QuantSeq

Summary

- Increasing atmospheric CO_2 levels have a variety of effects that can influence plant responses to microbial pathogens. However, these responses are varied, and it is challenging to predict how elevated CO_2 (*e*CO_2) will affect a particular plant-pathogen interaction. We investigated how *e*CO_2 may influence disease development and responses to diverse pathogens in the major oilseed crop, soybean (*Glycine max* [L.] Merr.).
- Soybeans grown in ambient CO_2 (*a*CO_2, 419 parts per million (ppm)) or in *e*CO_2 (550 ppm) were challenged with bacterial, viral, fungal, and oomycete pathogens, and disease, pathogen growth, gene expression and molecular plant defense responses were quantified.
- In *e*CO_2, plants were less susceptible to *Pseudomonas syringae* pv. *glycinea* (*Psg*) but more susceptible to bean pod mottle virus, soybean mosaic virus, and *Fusarium virguliforme*. Susceptibility to *Pythium sylvaticum* was unchanged, although a greater loss in biomass occurred in *e*CO_2. Reduced susceptibility to *Psg* was associated with enhanced defense responses. Increased susceptibility to the viruses was associated with reduced expression of antiviral defenses.
- This work provides a foundation for understanding of how future *e*CO_2 levels may impact molecular responses to pathogen challenge in soybean and demonstrates that agents infecting both shoots and roots are of potential concern in future climatic conditions.

Introduction

Atmospheric carbon dioxide (CO_2) levels are steadily rising and by some estimates, are predicted to increase to 550 parts per million (ppm) or more by mid-century. Increasing CO_2 levels, in combination with more extreme and unpredictable weather events, are expected to have significant impacts on global food security. The majority of plants on Earth use C3 photosynthesis, with relative atmospheric [O_2] and [CO_2] favoring photorespiration or photosynthesis, respectively (Pinto *et al.*, 2014). As a result, elevated CO_2 (*e*CO_2) stimulates photosynthesis, generally increasing plant biomass and yield, providing a potential benefit to crop production (Dusenge *et al.*, 2019; Ainsworth & Long, 2021). However, this CO_2 "fertilization effect" depends on a number of factors, including water and nutrient availability and optimal growth temperatures (Ainsworth & Long, 2021). Moreover, suppression of photorespiration, once thought to be a wasteful process, has been associated with poor growth (Timm & Bauwe, 2013), lower nutrient and protein content (Taub *et al.*, 2008; Broberg *et al.*, 2017), and reduced abiotic stress tolerance (Voss *et al.*, 2013) under ambient atmospheric conditions (*a*CO_2).

Another possible impact of *e*CO_2 is changes in the occurrence and severity of plant diseases. Pests and diseases that affect plant quality and yield pose one of the greatest challenges to crop production and are responsible for 17-30% of total yield losses of major crops (Savary *et al.*, 2019). Climate change is expected to cause latitudinal shifts in disease pressure associated with the migration of important plant pathogens to new geographic regions (Bebber *et al.*, 2013; Chakraborty, 2013; Raza and Bebber, 2022) as well as changes in pathogen virulence or aggressiveness (Pangga *et al.*, 2007; Lake & Wade, 2009; Aguilar *et al.*, 2015; Singh *et al.*, 2023). Additionally, *e*CO_2 has been demonstrated to alter interactions between plants and their attackers through changes in plant architecture, physiology, and molecular defense responses (Velásquez *et al.*, 2018; Bazinet *et al.*, 2022).

Plant disease development relies on three factors: a susceptible plant host, a virulent pathogen, and environmental conditions conducive to infection (Grulke, 2011). Over the past decade, tremendous advances have been made in our understanding of plant-microbe interactions (Ngou *et al.*, 2022; Petre *et al.*, 2022), however, it is still not well understood how changes in environmental conditions shape these interactions. Several mechanisms by which *e*CO_2 affects defense responses have been reported, including changes in leaf nutrition (Ryalls *et al.*, 2015; Sun *et al.*, 2016), stomatal density (Li *et al.*, 2015; Zhou *et al.*, 2017), host metabolism (Matros *et al.*, 2006; Ode *et al.*, 2014), and redox homeostasis (Mhamdi & Noctor,

82 2016; Noctor & Mhamdi, 2017; Foyer & Noctor, 2020; Ahammed & Li, 2022). Altered levels of
83 defense-related phytohormones, salicylic acid (SA), jasmonic acid (JA), and ethylene (ET), have
84 also been reported (Zhang *et al.*, 2015; Pan *et al.*, 2019; Zhou *et al.*, 2019). In general,
85 constitutive and/or pathogen-induced SA levels are higher in the foliar tissues of C3 plants grown
86 under *e*CO_2 (Bazinet *et al.*, 2022), suggesting increased resistance to viral and biotrophic
87 pathogens (Vlot *et al.*, 2009; Murphy *et al.*, 2020). However, the extent and directionality of these
88 responses are highly variable between studies (Bazinet *et al.*, 2022), which may reflect species,
89 cultivar or ecotype-specific CO_2 adaptations, as well as differences in additional environmental
90 growth conditions. For example, in tomato (*Solanum lycopersicum*), *e*CO_2 increased SA
91 biosynthesis, and plants displayed higher resistance to leaf curl virus, tobacco mosaic virus, and
92 the hemibiotrophic bacterial pathogen *Pseudomonas syringae* pv. *tomato* (*Pto*DC3000), but
93 were more susceptible to the necrotrophic fungal pathogen *Botrytis cinerea* (Huang *et al.*, 2012;
94 Zhang *et al.*, 2015). In contrast, *e*CO_2 increased JA-dependent responses in Arabidopsis
95 (*Arabidopsis thaliana*), enhancing resistance to *B. cinerea* and reducing resistance to
96 *Pto*DC3000 (Zhou *et al.*, 2019). These discrepancies highlight the need for direct investigations
97 of pathosystems involving important crop species rather than relying on generalized information
98 from model systems.

99 Soybean (*Glycine max* [L.] Merr.) is the most widely grown protein and oilseed crop,
100 accounting for approximately 329 million tons of global crop production in 2022
101 (http://www.worldagriculturalproduction.com/). The effect of *e*CO_2 on soybean physiology has
102 been investigated at various scales (Ainsworth & Long, 2021; Li *et al.*, 2021). In general, soybean
103 yield potential and root nodule mass increase under *e*CO_2 (Dermody *et al.*, 2008) with no
104 significant impact on plant nutrient or protein content (Myers *et al.*, 2014). *e*CO_2 has also been
105 associated with changes in leaf endophyte communities (Gonçalves *et al.*, 2021; Christian *et al.*,
106 2021), rhizospheric bacterial communities (Yu *et al.*, 2016), and responses to herbivore attack
107 (Casteel *et al.*, 2008; O'Neill *et al.*, 2010; Paulo *et al.*, 2020). However, only one study has
108 reported the effect of predicted future atmospheric conditions on soybean diseases by
109 monitoring the incidence and severity of some naturally occurring diseases at the Soybean Free
110 Air Concentration Enrichment (SoyFACE) facility (Eastburn *et al.*, 2010; Aspray *et al.*, 2023). As
111 soybean is susceptible to numerous economically important pathogens, including bacteria, fungi,
112 oomycetes, viruses, and nematodes (Whitham *et al.*, 2016), a formal investigation of how *e*CO_2
113 impacts susceptibility to diverse pathogens is needed. Moreover, the effect of *e*CO_2 on molecular
114 defense responses has not yet been investigated in this species.

115 In the present study, we compared the effects of CO_2 levels on soybean defense
116 response in plants grown under the current [*a*CO_2] of 419 parts per million (ppm) versus an
117 [*e*CO_2] of 550 ppm. Using the soybean-*P. syringae* pathosystem, we assessed innate immune
118 responses and disease susceptibility and conducted transcriptomic analyses to gain a global
119 understanding of how *a*CO_2 levels affect interactions in this pathosystem. We also conducted
120 infection experiments using two foliar viral pathogens, bean pod mottle virus (BPMV) and
121 soybean mosaic virus (SMV), and two filamentous root pathogens, *Fusarium virguliforme* and
122 *Pythium sylvaticum*, and demonstrate that *e*CO_2 exerts differential effects on interactions with
123 these diverse microbial pathogens. Our work provides a foundation for future studies
124 investigating the molecular interplay that regulates defense responses to *e*CO_2 and identifies
125 pathogens of potential concern in predicted future atmospheric conditions.

126 Materials and Methods

127 Plant growth and maintenance

128 Soybean (*G. max* cv. Williams 82) plants were grown in controlled environment chambers at the
129 Iowa State University Enviratron facility (Bao *et al.*, 2019) with lighting, humidity, and
130 temperature conditions as illustrated in Figure S1. [CO_2] maintained at 419 ppm represented
131 *a*CO_2 and 550 ppm represented future atmospheric conditions that may be reached by 2050
132 (*e*CO_2) (Jaggard *et al.*, 2010). For each condition, three replicate growth chambers were used
133 to provide biological replicates. Plants were grown in LC-1 potting soil mix (Sungro) and fertilized
134 weekly with 15-5-15 Cal-Mag Special (Peters Excel, G99140).

135 Physiological Measurements

136 To assess changes in soybean physiology associated with *e*CO_2, shoot biomass, photosystem
137 II (PSII) activity (quantum yield of fluorescence; ΦPSII activity) and stomatal conductance (gas
138 exchange rate; g_{sw}) were measured for 15 plants per CO_2 treatment. ΦPSII and g_{sw} were
139 obtained using a LI-600 Portable System (LI-COR Biosciences, Lincoln, NE, USA) during the
140 VC-V4 growth stages (Kumudini, 2010). ΦPSII measurements were conducted on the adaxial
141 surface of unifoliate leaves of 2-week-old plants and the newest fully expanded trifoliolate leaves
142 of 3- and 5-week-old plants. g_{sw} measurements were simultaneously collected from the abaxial
143 surface. At 21 days after planting (dap), leaves were collected from eight plants per treatment

144 and chamber, yielding three biological replicates per treatment for QuantSeq analyses (48
145 samples for QuantSeq dataset 1). Samples were collected between 09:00 and 10:00 am for all
146 replicates. At 35 dap, shoots were collected to determine fresh weight and dry weight.

147 Stomatal density, aperture, and index measurements

148 Stomatal density and aperture measurements were assessed from 10 leaf samples, while
149 stomatal index measurements were taken from five leaf samples for each CO_2 treatment at 21
150 dap. Impressions were made from the abaxial leaf surfaces using clear nail varnish (Ceulemans
151 *et al.*, 1995). Stomata were imaged using light microscopy, and counted in three randomly
152 selected fields of view per leaf sample. Stomatal aperture and stomatal index measurements
153 were conducted as described previously (Zhu *et al.*, 2021; Sultana *et al.*, 2021).

154 RT-PCR and RT-qPCR analysis

155 Total RNA was isolated from approximately 50 mg of leaf tissue using TRIzol Reagent (Thermo
156 Fisher Scientific, Waltham, MA, USA). Subsequently, 2 µg of RNA was reverse transcribed using
157 the Maxima First Strand cDNA Synthesis Kit (Thermo Fisher Scientific, Waltham, MA, USA).
158 Real-time quantitative PCR (RT-qPCR) was conducted using 2X PrimeTime Gene Expression
159 Master Mix (Integrated DNA Technologies, Coralville, IA, USA) and multiplexed probes designed
160 for *Pathogenesis-Related Protein 1* (*PR1*) (Glyma.13G251600), *Kunitz Trypsin Inhibitor 1* (*KTI1*)
161 (Glyma.08G342000), BPMV, or SMV (Table S1). Expression of *Dicer-Like 2* (*DCL2*)
162 (Glyma.09g025300) and *Argonaute 1* (*AGO1*) (Glyma.09g167100) was assessed using iTaq
163 Universal SYBR Green Supermix (BioRad, Hercules, CA, USA). To quantify *F. virguliforme* and
164 *P. sylvaticum*, soybean roots were collected at 14 and 35 dap, respectively. DNA was extracted
165 using the CTAB method (Rogers & Bendich, 1994), and RT-qPCR was performed using primers
166 specific to each pathogen (Table S1). *S-phase kinase-associated protein 1* (*Skp1*)
167 (Glyma.08G211200) was used as an internal reference for all experiments (Beyer *et al.*, 2021).
168 Primers and probes were designed from cultivar Williams 82 reference sequence (version
169 Wm82.a4.v1, (Schmutz *et al.*, 2010)) using PrimerQuest Tool (Integrated DNA Technologies).

170 Immune signaling assays

171 Oxidative species production was monitored in two-week-old soybean plants, as described
172 previously (Bredow *et al.*, 2019) using leaf discs collected from 16 plants per CO_2 treatment. The

173 elicitor solution contained 100 μM luminol (Sigma-Aldrich, St. Louis, MO), 10 μg/mL horseradish
174 peroxidase (Sigma-Aldrich, St. Louis, MO), with or without 100 nM flg22 (VWR International,
175 Radnor, PA). Chemiluminescence was quantified on a GloMax® plate reader (luminescence
176 module; Promega, Madison, WI) every 2 min for 30 min with a 1000 ms integration time.
177 Flg22-induced MITOGEN-ACTIVATED PROTEIN KINASE (MAPK) activation was
178 assessed as described previously (Xu *et al.*, 2018) using leaf discs collected from six plants per
179 CO_2 treatment. Leaf discs were maintained in CO_2 chambers, treated with 100 μM of flg22
180 peptide and sampled between 0 and 250 min. Total protein was extracted and normalized as
181 described previously (Wang *et al.*, 2018) and MAPK activation was assessed by immunoblot
182 analysis using primary anti-Phospho-p44/42 MAPK antibody (Erk1/I 2; Thr-202/Tyr-204) (Cell
183 Signaling, Danvers, MA, USA) and secondary goat anti-rabbit-HRP antibody (Cell Signaling,
184 Danvers, MA, USA).

185 Bacterial infection assays

186

187 *P. syringae* pv. *glycinea* (*Psg*), *Pto*DC3000, and *Pto*DC3000 *hrcC-* (*hrcC-*), were grown at 30°C
188 overnight in Luria Bertani (LB) broth with appropriate antibiotics. The next day, cells were
189 harvested and resuspended in 10 mM $MgCl_2$ at OD_{600}=0.2 (1 x 10^8 colony forming units
190 (CFU)/mL). Immediately before inoculations, 0.04% of Silwet L-77 (ThermoFisher Scientific,
191 Waltham, MA) was added to the suspension, and the unifoliate leaves of 14-day-old soybeans
192 were spray-inoculated on adaxial and abaxial surfaces until fully wet. Leaf discs were extracted
193 from 24 plants per treatment, between 1- and 7-days post-infection (dpi). Leaf discs from three
194 plants were pooled per sample, and were used to quantify CFU/cm^2 as previously described (Liu
195 *et al.*, 2015). For phytohormone analysis, eight plants per treatment were sampled at 6- and 24-
196 hours post-infection (hpi) and QuantSeq was performed using 6 hpi samples. g_{sw} in response to
197 *Psg* was measured at 1 hpi using 10 plants per treatment. For QuantSeq analyses, leaves were
198 collected from eight *Psg*-infected and mock-infected plants per CO_2 treatment and chamber,
199 yielding three biological replicates per treatment for QuantSeq analyses (96 samples, QuantSeq
200 dataset 2). Samples were collected between 09:00 and 10:00 h for all replicates.

201 ## Bacterial growth curves

202 *Pto*DC3000 cultures were inoculated to a starting concentration of 1 x 10^7 CFU/mL in 100 mL of
203 LB broth containing appropriate antibiotics. Cultures were grown in temperature-controlled
204 growth chambers maintained at 28°C (no light), ~20% relative humidity, and either 419 or 550
205 ppm of CO_2. Cultures were shaken at 100 rpm and OD_{600} was recorded every four hours over
206 32 hours.

207 ## QuantSeq

208 Total RNA was extracted from 50 mg of soybean leaf tissue using the Direct-zol RNA Miniprep
209 Plus Kit with DNaseI treatment (Zymo Research, Irvine, CA). RNA samples were quantified
210 using a Qubit 4.0 Fluorometer (Invitrogen, Carlsbad, CA), and RNA integrity was assessed using
211 the Fragment Analyzer Automated CE System. All RNA samples used for sequencing had an
212 RQN (RNA Quality Number) equal to or greater than 7. Library preparation was performed using
213 the QuantSeq 3' mRNA-Seq Library Prep Kits (Lexogen, Greenland, NH), and samples were
214 sequenced using the Illumina NovaSeq 6000 System (Iowa State University DNA Facility).

215 ## Bioinformatic and Statistical Analysis of QuantSeq data

216 For each of the QuantSeq datasets (48 and 96 libraries), libraries were each sequenced on two
217 lanes, generating two sequence files per library. Files were inspected with FASTQC (de Sena
218 Brandine & Smith, 2019) to confirm sequence quality and quantity. Trimmomatic was used to
219 remove adaptor sequences, low quality bases and reads less than 50 bp in length (Bolger *et al.*,
220 2014). STAR version 2.7.10 (Dobin *et al.*, 2013) was used to align reads to the Williams 82
221 reference genome sequence (Wm82.a4, (Schmutz *et al.*, 2010)). Samtools version 1.17 (Li *et*
222 *al.*, 2009) was used to merge read data from separate lanes and identify uniquely mapping reads
223 within the combined mapping files (bam files). Mapping files were imported into RStudio version
224 4.2.3 (Dobin *et al.*, 2013) using Rsamtools (Morgan *et al.,* 2021). The gene feature file (GFF)
225 corresponding to the reference genome was imported using rtracklayer (Lawrence *et al.*, 2009).
226 The number of reads per sample aligning to each gene was counted using summarizeOverlaps
227 and a count table for all expressed genes within a tissue was generated. Over 329 million and
228 659 million uniquely mapping reads were identified across QuantSeq datasets 1 and 2,
229 respectively. Data were normalized using the Trimmed Mean of M values (Gupta *et al.*, 2021) in

230 the Bioconductor package edgeR (Robinson & Smyth, 2007; Robinson *et al.*, 2010; McCarthy
231 *et al.*, 2012; Zhou *et al.*, 2014). Only genes with log2 counts per million (cpm) > 1 in at least
232 three replicates were used in the analysis. ggplot2 (Wickham, 2009) was used to generate
233 principal component, biological coefficient of variance, and MA plots to visually compare sample
234 replicates and ensure reproducibility (Dziuda, 2010). Two and eight libraries with less than 1
235 million uniquely mapping reads were removed from subsequent analyses from QuantSeq
236 datasets 1 and 2, respectively, leaving a minimum of six plant replicates per condition. Following
237 renormalization, edgeR was used to analyze differentially expressed genes (DEGs) among the
238 different datasets. For QuantSeq dataset 1, we identified DEGs whose expression changed in
239 response to CO_2 levels (*e*CO_2 levels/*a*CO_2) at 21 days using a false discovery rate (FDR) < 0.01.
240 For QuantSeq dataset 2, we identified DEGs responding to *Psg* treatment (*Psg*/mock) in control
241 and *e*CO_2 conditions and DEGs whose expression changed in response to CO_2 in *Psg*-treated
242 (*Psg e*CO_2/*Psg* control CO_2) or mock-treated samples (Mock *e*CO_2/*a*CO_2) using an FDR < 0.01.
243 Hierarchical clustering in RStudio using hclust (Murtagh, 1985) was used to group similarly
244 expressed genes from DEG lists of interest. Heatmaps were generated using Heatmap.2 in
245 ggplot2 (Wickham, 2009).

246 DEG Annotation and Analysis of Overrepresented Transcription Factors 247 and Promoters

248 DEGs were annotated using the SoyBase Gene Annotation Lookup Tool for Wm82.a4
249 (https://www.soybase.org/genomeannotation/). For given DEGs of interest, the best BLASTP
250 Arabidopsis hits (TAIR version 10) from the annotation were used to query the STRING database
251 (Szklarczyk *et al.*, 2023). To identify transcription factors (TFs) within DEG lists of interest, we
252 used custom perl scripts to query *G. max* transcription factor information downloaded from the
253 Plant Transcriptional Regulatory Map/Plant Transcription Factor Database
254 (PlantRegMap/PlantTFDB v5.0, (Tian *et al.*, 2020), https://plantregmap.gao-lab.org). To identify
255 TF binding sites significantly overrepresented within promoters of DEGs of interest we used the
256 PlantRegMap TF enrichment tool (https://plantregmap.gao-lab.org/tf_enrichment.
257 php) for *G. max*, using all available methods and threshold p-value < 0.05.

258 ## Single Phase Extraction for JA-Targeted and SA (Non-Targeted)
259 ## Metabolomic Analyses

260 Approximately 100 mg of each sample was ground and spiked with an internal standard
261 containing 10 µg nonadecanoic acid (1 mg/mL in ethanol) and JA-d5 (Cayman Chemical, Ann
262 Arbor, MI) (JA-d5) (2.5 µg/mL in ethyl acetate). The extraction was initiated with the addition of
263 90% ice cold methanol using a modified version of the methanolic extraction protocol established
264 previously (Jiye *et al.*, 2005).

265 ## GC-MS Acquisition and Analysis for SA

266 Six hundred microliters of the combined extracts were aliquoted and dried using a speed-vac
267 concentrator for 10 hours and then derivatized according to established protocols (Koek *et al.*,
268 2006). Gas Chromatography Mass Spectrometry (GC-MS) analysis was performed with an
269 Agilent 6890 gas chromatograph coupled to a model 5973 Mass Selective Detector (Agilent
270 Technologies, Santa Clara, CA) using a HP-5MSI 5% phenyl methyl silox with 30 m × 250 µM ×
271 0.25 µm film thickness (Agilent Technologies). Identification and quantification were conducted
272 using AMDIS (Automated Mass spectral Deconvolution and Identification System, National
273 Institute of Standards and Technology, Gaithersburg, MD) with a manually curated, retention
274 indexed GC-MS library with additional identification performed using the NIST20 and Wiley 11
275 GC-MS spectral library (Agilent Technologies, Santa Clara, CA). Final quantification was
276 calculated by integrating the corresponding peak areas relative to the area of the nonadecanoic
277 acid internal standard. Raw data were normalized to the amount of tissue used.

278 ## LC-MS Acquisition for Targeted JA Analysis

279 An Oasis Hydrophilic-Lipophilic-Balanced (HLB) column (30 mg sorbent) (Waters Corporation,
280 Milford, MA) was used for the purification of JA as established previously (Kojima *et al.*, 2009;
281 Kojima & Sakakibara, 2012). Liquid chromatography (LC) separations were performed with an
282 Agilent Technologies 1290 Infinity II UHPLC instrument equipped with an Agilent Technologies
283 ZORBAX Eclipse C18 (1.8 µm 2.1 mm × 100 mm) analytical column that was coupled to a 6470
284 triple quadrupole mass spectrometer with an electrospray ionization source (Agilent
285 Technologies, Santa Clara, CA). A volume of 20 µL of each sample was injected into the LC
286 system with the mass spectrometer in negative mode. Multiple reaction monitoring (MRM) was

287 used for detection with transitions of m/z 209→59 (JA) and 214→62 (JA -d5), with fragmentation

288 conducted at 25 eV for both JA and JA-d5.

289 Viral infection assays

290 Lyophilized soybean leaves infected with BPMV or SMV were ground in 10 mL of 50 mM
291 potassium phosphate buffer (pH 7.5) per 1 g of tissue. One unifoliate leaf of 14 dap soybean
292 was dusted with carborundum (Fisher Scientific, Waltham, MA) and rub-inoculated with 50 µL of
293 inoculum or buffer (mock). The second unifoliate leaf was inoculated two days later using the
294 same method. Systemic leaves were sampled from six plants per treatment, at 14 and 21 dpi to
295 assess viral titer. Fresh weight, dry weight, and gene expression were measured using 21 dpi
296 plants. Disease severity was evaluated between 0 and 21 dpi using a single-digit disease rating
297 scale ranging from 0 to 3 (0 = no disease, 1 = mild, 2 = moderate, and 3 = severe). Area under
298 disease progress curve (AUDPC) was calculated based on the equation below (Simko & Piepho,
299 2012).

300 $$AUDPC = \sum_{i=1}^{n-1} \left[\frac{D_{(i+1)} + D_i}{2}\right] [T_{i+1} - T_i]$$

301 Di = disease severity on ith date, Ti = ith date, and n = total number of observations

302 *F. virguliforme* and *P. sylvaticum* infection assays

303 Sterilized sorghum (*Sorghum bicolor*) seeds were inoculated with *F. virguliforme* (isolate
304 LL0036) and incubated in the dark at room temperature for 21 days and dried for 3-4 days.
305 Styrofoam cups (8 oz.) were filled with a mixture of 180 mL of sterile sand soil and 9 mL of *F.*
306 *virguliforme*-infested sorghum. Soybean seeds were placed in the cup and covered with 25 mL
307 of peat mix. At 35 dap, roots and shoots were sampled from six cups of each CO_2 treatment to
308 measure fresh weight and dry weight. Disease severity was assessed on leaves on a 0 to 7
309 rating scale as described (Roth *et al.*, 2019) (Table S2), and the AUDPC was calculated. For
310 plate growth assays, a starting culture of *F. virguliforme* was prepared on 1/3 strength potato
311 dextrose agar (PDA) and grown at room temperature for 21 days in the dark. A 7-mm plug was
312 punched out of the starting culture and placed into the center of a 90-mm-diameter Petri dish
313 containing 1/3 strength PDA. Ten plates per CO_2 treatment were maintained in the dark under
314 *a*CO_2 or *e*CO_2. Fungal growth was assessed every other day for 11 days.

315 Millet was inoculated with a 3-day-old culture of *P. sylvaticum* and incubated in the dark
316 at room temperature for 7-14 days (Matthiesen *et al.*, 2016). A mixture of 100 mL of sterile sand
317 soil and 5 mL of *P. sylvaticum*-infested millet was placed in a 237 mL (8 oz.) polystyrene cup
318 and covered with 25 mL of peat mix. The seed was placed on top of the peat mix and then
319 covered with another 25 ml layer of peat mix. At 14 dap, plants in six cups of each treatment
320 were up-rooted, roots were washed, and disease severity was assessed using a 0 to 4 rating
321 scale adapted from (Zhang & Yang, 2000) (Table S3). Root and shoot fresh weight and *P.*
322 *sylvaticum* copy numbers were determined at 21 dap. For plate growth assays, a starting culture
323 of *P. sylvaticum* (isolate Gr8) was grown on 1/2 strength PDA at room temperature for 5 days in
324 the dark. A 7-mm plug was punched and transferred into the edge of a 90-mm-diameter Petri
325 dish containing 1⁄2 strength PDA. Ten plates per treatment were incubated in the dark under
326 *a*CO_2 or *e*CO_2. Oomycete growth was measured from the edge of the inoculum plug to the tip of
327 the longest hypha and was assessed every 24 h for 96 h.

328 Statistical analysis

329 Linear mixed-effects models (LMM) were fit to each response following the experimental design.
330 Taking the bacterial infection experiment measuring CFUs as an example, the whole-plot factor
331 was CO_2 level and the whole-plot experimental units were growth chambers. Randomized
332 complete block design was implemented at the whole-plot level, with each block comprising a
333 pair of chambers at *a*CO_2 or *e*CO_2. At the split-plot level, 24 plants were assigned to each
334 pathogen, with sets of three plants pooled for each CFU measurement, repeated over time.
335 Following this split-plot design, the fixed effects of the LMM include the main effects and all
336 interaction effects of the factors CO_2, bacterial species, and time, and random effects include
337 block, chamber, split-plot, and sets of plants. Similar to this example, LMMs were fit for other
338 responses following the corresponding experimental designs.
339 For response variables that exhibited unequal variances on the original scale, LMM
340 analysis was done on power- or log- transformed data, and the Delta method was used to
341 compute standard errors for the original scale. For all LMM analysis, model diagnostic checks
342 were done to ensure that model assumptions were appropriate. Parameters of LMM were
343 estimated using lmer() in the lme4 R package. The emmeans() function in the emmeans R
344 package was used to compute the SE. Type III ANOVA tables with F tests were conducted by
345 anova() and the lmerTest R package.

Results

Elevated CO_2 alters soybean physiology and gene expression

Prior to studying the effects of *e*CO_2 on soybean defense, we wanted to ensure that our growth conditions caused changes in physiological responses that were previously observed under higher atmospheric CO_2 (Ainsworth & Long, 2021; Li *et al.*, 2021). At 14 dap, soybean plants grown in *e*CO_2 displayed no difference in ΦPSII activity compared to plants grown at *a*CO_2 (Figure 1a). However, at 21 and 35 dap, ΦPSII activity was higher in *e*CO_2 (Figure 1a), indicating a higher photosynthetic rate. Stomatal conductance to water vapour (g_{sw}) was also affected, with plants grown at *e*CO_2 displaying lower g_{sw} at 21 and 35 dap (Figure 1b), which was consistent with the lower stomatal density (Figure 1c) and reduced stomatal aperture (Figure 1d) on the abaxial leaf surface. In line with the lower stomatal density, a reduction in stomatal index was observed at *e*CO_2, indicating that the decrease in stomatal density was due to reduced stomatal production and not an increase in leaf expansion (Figure S2). At 35 dap, soybeans grown in *e*CO_2 had greater shoot fresh weight (Figure 1e) and dry weight (Figure 1f) and were visibly larger than those grown in *a*CO_2 (Figure 1g). Together, these experiments demonstrate that a 31% increase in [CO_2] induced physiological responses under our conditions that were consistent with prior studies.

To investigate gene expression changes associated with physiological responses to *e*CO_2, we conducted QuantSeq analysis using RNA isolated from unifoliate leaves at 21 dap. We identified 388 DEGs (Table S4), which were used to construct a heat map that formed two distinct clusters associated with [CO_2] (Figure 2a). The 180 DEGs in cluster 1 were repressed in *e*CO_2, while the 208 DEGs in cluster 2 were induced in *e*CO_2 (Table S4). To identify gene networks responding to [CO_2], the 321 best BLASTP Arabidopsis homologs corresponding to our 388 soybean DEGs were were used as input for STRING (Szklarczyk *et al.*, 2023) and gene ontology (GO) analyses (Szklarczyk *et al.*, 2023) to identify biological processes (BP) that were overrepresented within each cluster (Table S5). In cluster 1, two major themes emerge related to i) responses to JA signaling (*e.g.* response to wounding, response to hormone, regulation of defense response, response to lipid, regulation of JA-mediated signaling) and ii) photosynthesis

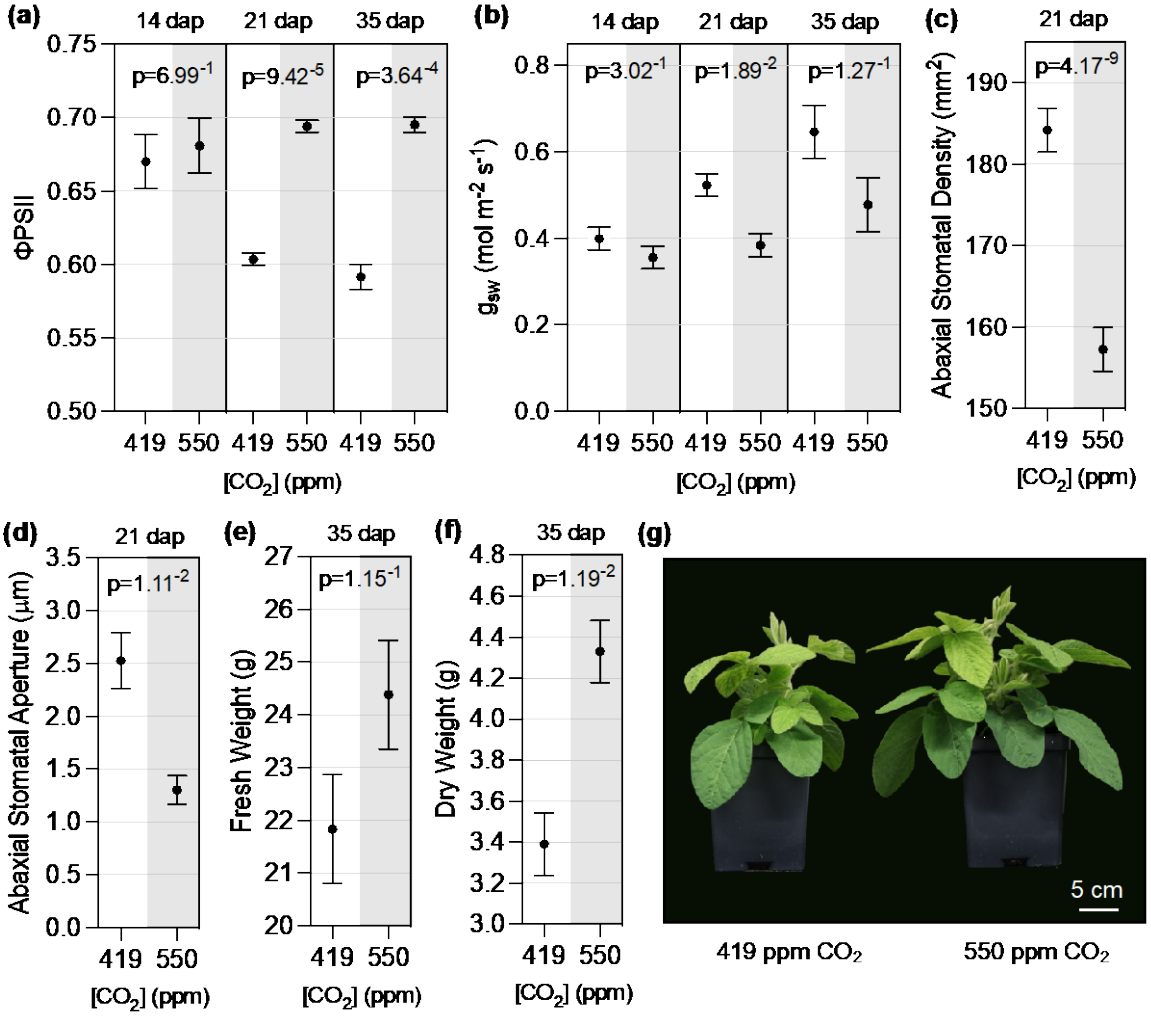

Figure 1. Effects of eCO_2 on soybean physiology and growth. (a) Photosystem II (ΦPSII) activity and **(b)** stomatal conductance (g_{sw}) were measured at the indicated days after planting (dap) using a LI-600 portable system. **(c)** Stomatal density and **(d)** stomatal aperture measured at 21 dap using three randomly selected fields of view per leaf sample using a brightfield microscope. **(e)** Shoot fresh weight, **(f)** shoot dry weight, and **(g)** representative photos of soybean plants at 35 dap. All measurements and samples were taken from the newest fully expanded leaves of 10 plants at each time point, except ΦPSII and g_{sw}, which were measured in 15 plants per CO_2 treatment. The three experimental replicates were conducted simultaneously in independent CO_2 controlled chambers using a replicated completely randomized design. Data was graphed as the mean across the three replicates with standard error bars. Linear mixed effect model (LMM) analysis was applied to the fourth power of ΦPSII 35 dap and log-transformed stomatal aperture data due to unequal variance on the original scale. P-values were computed based on F-tests for the effect of CO_2 at each time point from the LMM analysis.

391
392
393
394
395

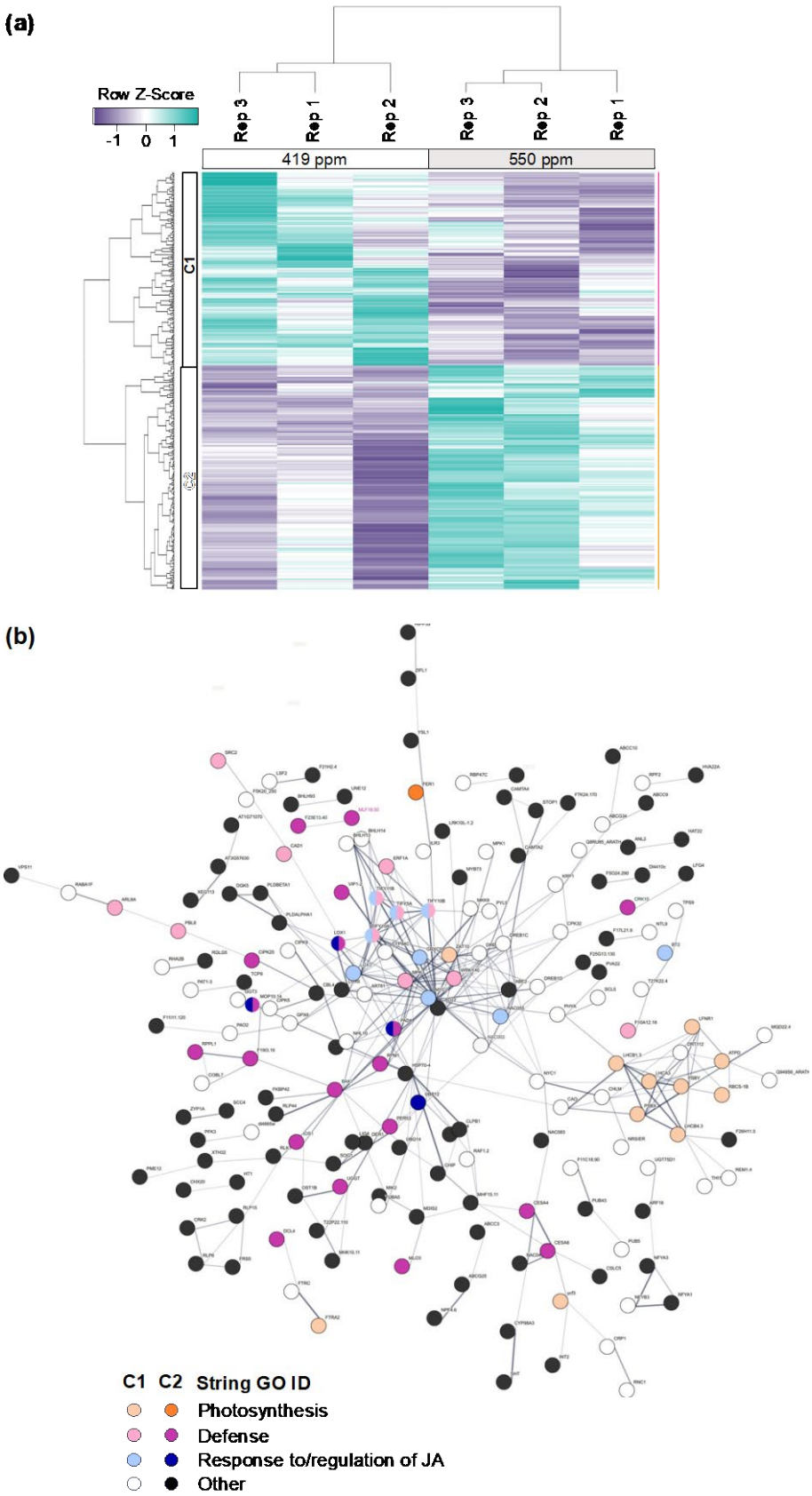

Figure 2. Transcriptomic analysis of soybean gene expression in leaves of plants grown under *a*CO_2 (419 ppm) or *e*CO_2 (550 ppm). (a) DEGs responding to eCO_2 were identified using a FDR < 0.01 (Table S3). Samples for QuantSeq analysis were taken from the newest fully expanded leaves of soybean plants at 21 days after planting. The three experimental replicates were conducted simultaneously in independent CO_2 controlled chambers using eight plants per CO_2 treatment. Row Z-scores were used for hierarchical clustering of DEGs, based on expression across samples and replicates. Two expression clusters were identified. DEGs in cluster 1 were expressed at higher levels in 419 ppm vs 550 ppm CO_2 and DEGs in cluster 2 were expressed at higher levels in 550 ppm vs 419 ppm CO_2. **(b)** STRING network for DEGs identified between *a*CO_2 and *e*CO_2 in leaves at 21 (dap). The 388 genes identified in soybean correspond to 321 genes in *Arabidopsis thaliana* that were used to assign functional annotations. Lightly shaded or white circles indicate DEGs from cluster 1 (C1) and brightly shaded and black circles indicate DEGs from cluster 2 (C2).

(*e.g.* response to light intensity, response to high light intensity, photosynthesis, photosynthesis light reaction). The STRING association network produced from the genes in cluster 1 also highlights the effects on JA signaling with a node of highly connected genes that include *MYC2* transcription factor and *TIFY* (JAZ repressor) genes (Figure 2b, light blue). A node of highly connected genes in the lower right quadrant includes several genes related to photosynthetic processes, including soybean homologs of *AtRbcS1B, AtRAF1, AtLHCB8, AtLHCB1, AtCHLM*, and *AtPIF1* (Figure 2b, light orange).

Major themes emerging from cluster 2 are BP terms related to i) defense (*e.g.* defense, response to external stimulus, response to biotic stimulus, response to bacterium, response to other organism) and ii) protein modification (*e.g.* protein phosphorylation, protein modification process, phosphorus metabolic process) (Table S5). The STRING association network identifies interconnected genes associated with defense responses (Figure 2b). These nodes include soybean homologs of *AtBAK1*, *AtPAD4*, and *AtIOS1* (Table S4), all required for pattern-triggered immunity (PTI) responses (Yeh *et al.*, 2016; Pruitt *et al.*, 2021), and a number of resistance-like proteins, including *AtRPM1*, *AtRLP1*, and *AtRLP44*. While not highlighted in the STRING analyses, soybean homologs of genes associated with reduced g_{sw} and stomatal aperture (*AtHT1*, *AtFER*, *AtZIFL1*, *AtPLDa1*, and *AtNRT1:2*) were upregulated in *e*CO_2 (Table S4). Together, our gene expression analyses indicate that *e*CO_2 causes changes in the transcriptome of unifoliate soybean leaves, repressing expression of photosynthetic genes, altering JA signaling, priming innate immunity against microbial pathogens and promoting expression of genes associated with stomatal closure.

431 ## Soybean resistance to *Pseudomonas spp.* is enhanced under *e*CO_2

432 In order to assess the impacts of *e*CO_2 on susceptibility to microbial pathogens, we first used
433 the well characterized soybean-*P. syringae* pathosystem (Lindeberg *et al.*, 2009; Whitham *et al.*,
434 2016). Basal defense against bacterial pathogens is initiated by cell surface receptors that
435 recognize microbe-associated molecular patterns (MAMPs), such as the bacterial flagellin
436 peptide flg22 (DeFalco & Zipfel, 2021). *Psg*, which causes bacterial blight in soybean, was
437 chosen to model a compatible interaction where effectors effectively suppress immunity resulting
438 in disease (Prom & Venette, 1997). At 1 dpi, the proliferation of *Psg* was 1.1-$\log_{10}$ fold lower in
439 plants grown in *e*CO_2 compared to *a*CO_2 (Figure 3a), and it remained significantly reduced in
440 *e*CO_2 over the 7-d time course (Figure 3a). In compatible interactions, *Psg* infection causes the
441 development of necrotic spots that become surrounded by yellow halos (Budde & Ullrich, 2000).
442 At 7 dpi, soybeans infected under [*a*CO_2] displayed necrotic lesions across the surface of leaves,
443 consistent with bacterial blight symptoms (Figure 3b). In contrast and consistent with reduced
444 *Psg* growth, few disease symptoms were observed on the leaves of plants grown at *e*CO_2
445 (Figure 3b).

446 We also inoculated plants with *Pto*DC3000, as an example of an incompatible interaction
447 causing hypersensitive cell death resulting in disease resistance (Whalen *et al.*, 1991), and the
448 *Pto*DC3000 type III secretion mutant, *hrcC-*, that cannot secrete bacterial effector proteins and
449 therefore cannot multiply or induce hypersensitive cell death (Brooks *et al.*, 2004). Lower CFUs
450 were consistently observed across the time course in soybean grown at *e*CO_2 when inoculated
451 with either *Pto*DC3000 or *hrcC-*, although the p-values were greater than 0.05 (Figure 3a). At 7
452 dpi, *Pto*DC3000-infected plants grown at either [CO_2] began to show signs of a hypersensitive
453 reaction while *hrcC-* infection did not result in obvious disease or defense phenotypes,
454 regardless of the [CO_2] (Figure 3b).

455 To assess if atmospheric [CO_2] independently affects bacterial growth rate, we conducted
456 a growth curve analysis on liquid cultures of *Pto*DC3000 in our controlled environment growth
457 chambers. The growth curves of *PtoDC3000* cultures were similar between the two CO_2 levels
458 (Figure S3), indicating that reduced growth of *P. syringae* in soybean is not due to direct effects
459 of *e*CO_2 on bacterial multiplication. Together, these data suggest that *e*CO_2 enhances resistance
460 to *P. syringae* infection in soybean during compatible interactions and, to a lesser extent, during
461 an incompatible interaction.
462

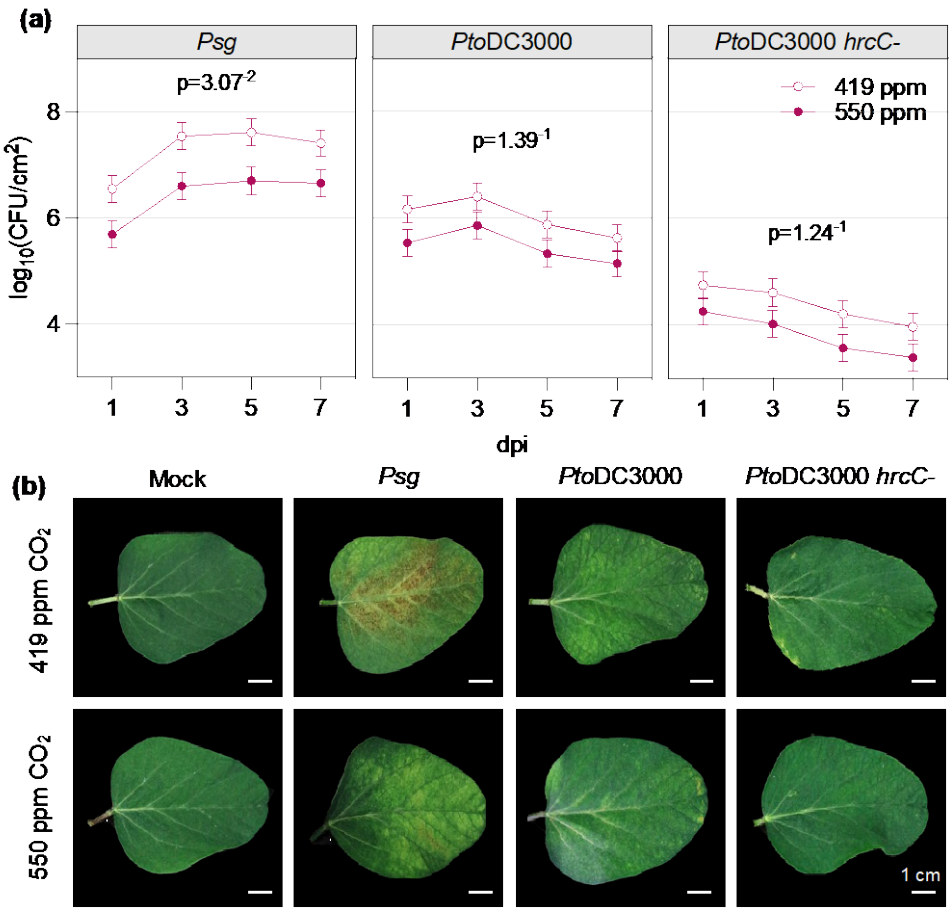

Figure 3. Soybean plants growing in *e*CO_2 are less susceptible to *P. syringae*. (a) Colony forming units (CFU) of *P. syringae* pv. *gycinea* (*Psg*), *P. syringae* pv. *tomato* (*Pto*DC3000) and *Pto*DC3000 *hrcC*$^-$ were quantified in the unifoliate leaves of plants at 1, 3, 5, and 7 days post-inoculation (dpi). The unifoliate leaves of 24 plants were sampled for each treatment group, and three independent biological replicates were performed. Data points represent the mean CFU count of the three biological replicates with standard error bars. P-values were computed using t-tests for the contrast between two CO_2 levels of each pathogen averaged over dpi from the LMM analysis. **(b)** Representative images of unifoliate leaves photographed at 7 dpi. Mock plants were treated with 10 mM $MgCl_2$, 0.04% Silwet L-77 solution with no bacteria.

Elevated CO_2 alters basal immune responses

To determine if *e*CO_2 affects immunity to *Psg* on a molecular level, we assessed multiple hallmarks of plant immune signaling. In response to *Psg*, the change in stomatal conductance following *Psg* treatment did not differ between [CO_2] (Figure 4a). However, soybeans grown at *e*CO_2 exhibited greater overall production of reactive oxygen species when considering both mock- and flg22-treated leaf discs (Figure 4b) as well as higher and more sustained MAPK activation (Figure 4c). We also observed that a soybean *PR1* homolog, an SA-regulated defense gene, accumulated to higher levels in mock- and *Psg*-inoculated plants grown in *e*CO_2,

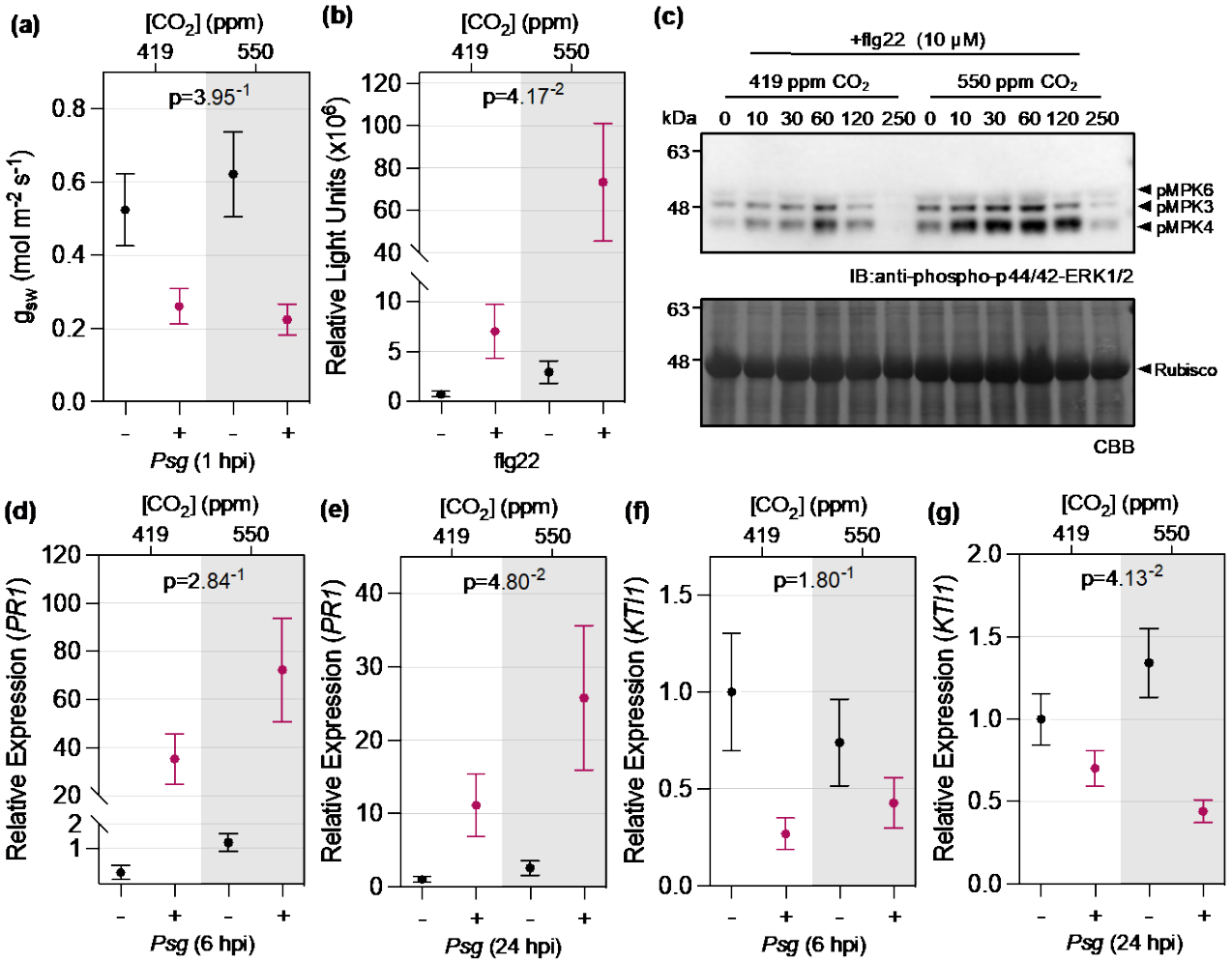

Figure 4. Bacterially-induced defense signaling is more strongly upregulated in soybean leaves grown under eCO2. (a) Stomatal conductance (g*sw*) at 1 hour post-inoculation (hpi) with *P. syringae* pv. *glycinea* (*Psg*). **(b)** Reactive oxygen species (ROS) production in response to bacterial flagellin 22 (flg22) peptide was quantified using a chemiluminescence assay. Relative light units were determined using leaf discs from 12 plants per treatment, and **(c)** flg22-induced MAPK activation using protein extracted from 12 plants per time point (0 to 250 minutes after treatment) and visualized by immunoblot analysis. Expression of *PR1* (SA marker gene) **(d)** 6 hpi and **(e)** 24 hpi and expression of *KTI1* (JA marker gene) **(f)** 6 hpi and **(g)** 24 hpi with *Psg* or mock treatment was assessed by RT-qPCR. RNA was extracted from six plants per treatment and expression was measured relative to the *Skp1* housekeeping gene. All experiments were conducted using leaves or leaf discs collected from 14-day old plants grown under 419 ppm or 550 ppm CO2. Three independent replicates were conducted for each experiment. Data points represent average values across the three experimental replicates with standard error bars. P-values for ROS production and *PR1* expression were computed using F-tests for the main effect of CO2 , and g*sw* and *KTI1* expression using the interaction effect between CO2 and *Psg*, from the LMM analysis based on log-transformed data.

particularly in the 24 hpi sample (Figure 4d,e) and corresponded to a slightly greater SA accumulation in leaves sampled at 6 hpi (Figure S4a). At 24 hpi, expression of the JA marker gene *KTI1* was more down regulated in response to *Psg* (Figure 4f,g). However, JA accumulation was not affected by [CO_2] in our metabolomics analysis (Figure S4b). Together,

505 these data suggest that bacterially-induced immune signaling is more robust in plants grown in
506 *e*CO_2, which correlates with the enhanced resistance to *Pseudomonas spp.* in these plants.

507 *e*CO_2 alters the soybean transcriptome in response to *Psg*

508 To gain further insight into the effects of *e*CO_2 on molecular responses to *Psg* treatment, we
509 conducted QuantSeq analysis on soybean leaves at 6 hpi with buffer alone (mock) or with *Psg*.
510 We identified DEGs in mock- versus *Psg*-treated plants grown at each of the two [CO_2]: 18,054
511 DEGs were identified in plants grown in *a*CO_2 and 19,443 DEGs were identified for plants grown
512 in *e*CO_2. We produced a combined list of all unique DEGs for a total of 21,822 *Psg*-responsive
513 DEGs, which was used to generate a heat map that formed four distinct clusters (Figure S5;
514 Table S6). Cluster 1 (1,661 DEGs) had mixed expression in response to *Psg* treatment and no
515 significantly (corrected $p<0.05$) overrepresented GO terms (Table S7). Cluster 2 (9,822 DEGs)
516 was induced by *Psg* treatment and had 81 significant GO terms associated with stress (response
517 to cadmium ion, heat, hypoxia, oxidative stress, salt, and UV-B), defense (response to chitin,
518 defense response to bacterium, fungus, and virus, cell death, regulation of SA biosynthesis,
519 response to SA, hypersensitive response, and systemic acquired resistance), and ER stress
520 (protein folding, response to unfolded protein, and response to ER stress). Clusters 3 (6,718
521 DEGs) and 4 (3,621 DEGs) were repressed by *Psg* treatment. While cluster 3 had 50 significant
522 GO terms associated with photosynthesis, response to light, and circadian rhythm, cluster 4 had
523 two significant GO terms: response to starvation and oxidation-reduction process. Among DEGs
524 repressed by *Psg* treatment in *a*CO_2 and *e*CO_2 conditions, 61.6% had greater negative fold-
525 changes in *e*CO_2 (7,419/12,053 DEGs). Similarly, for DEGs induced by *Psg* in *a*CO_2 and *e*CO_2
526 conditions, 60.1% had greater positive fold changes in soybeans grown in *e*CO_2 (5,671/9,357
527 DEGs).

528 To further understand how responses to *Psg* differ with changes in atmospheric [CO_2],
529 we identified 622 and 1,919 DEGs associated with *e*CO_2 versus *a*CO_2 in mock- or *Psg*-
530 inoculated plants, respectively (Table S8). Using a union of these two lists, we generated a
531 heatmap of the 2,419 DEGs, which formed five distinct clusters (Figure 5). To assign potential
532 function to each of the clusters, we used the Arabidopsis best BLASTP homologs corresponding
533 to all DEGs within a cluster as input into STRING (Szklarczyk *et al.*, 2023) and performed GO
534 BP enrichment for each cluster (Table S9). Cluster 1, which tended to be induced by *e*CO_2 in
535

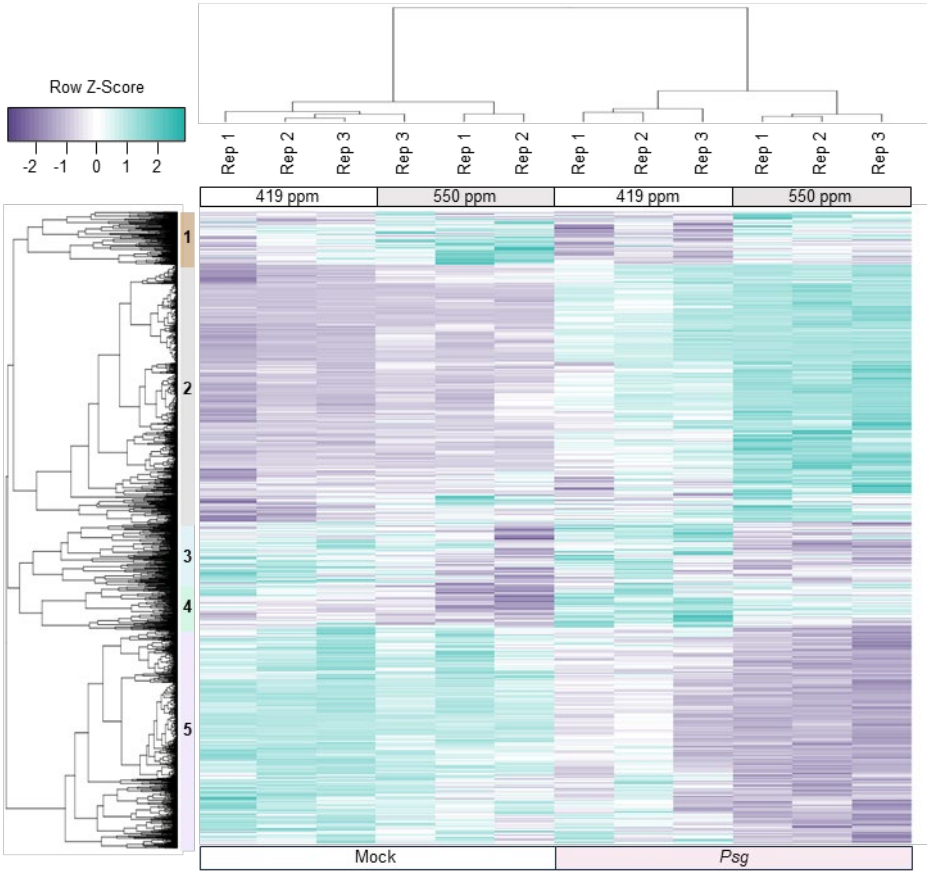

536
537 **Figure 5. Identification of soybean DEGs responding to eCO_2 (419 ppm versus 550 ppm) in either**
538 **mock or *Pseudomonas syringae* pv. *gylcinea (Psg*) infected samples at 6 hpi.** Samples for
539 QuantSeq analysis were taken from the unifoliate leaves of 14-day old plants at 6 h post-inoculation with
540 mock treatment or *Psg*. The three independent replicates were conducted using eight plants per CO_2
541 treatment. **(a)** Using an FDR < 0.01, we identified 2,419 DEGs responding to eCO2 in *Psg* and/or mock-
542 treated samples. Row Z-scores were used for hierarchical clustering of DEGs, based on expression
543 across samples and replicates. Purple indicates expression values below the row mean for a given DEG
544 and sample and teal indicates expression values above the row mean for a given DEG and sample. Rep
545 indicates the independent biological replicate. The five major expression clusters of DEGs are indicated
546 as 1 to 5, with clusters 2 and 5 containing the most genes. Cluster 2 contains 986 genes that are primarily
547 upregulated at 6 hpi with *Psg* but these genes are upregulated more in *e*CO_2. Cluster 5 contains 828
548 genes that are downregulated at 6 hpi with *Psg*, but these genes are more down regulated in *e*CO_2.
549
550
551 mock and *Psg* samples, was associated with 40 GO terms related to stress (response to
552 chemical, stress, and abiotic stimulus) and defense (regulation of JA signaling, response to JA,
553 response to bacterium, and defense response). DEGs in cluster 2 were induced by *Psg* with
554 greater induction observed in *e*CO_2 and corresponded to 139 significant GO terms related to
555 stress and defense responses. DEGs in cluster 3 were repressed by *e*CO_2 and corresponded to
556 37 significant GO terms, many associated with stress and regulation (regulation of transcription,
557 circadian rhythm, primary metabolism, development, and photoperiodism). DEGs in cluster 4
558 were induced by *Psg* with greater induction observed in *a*CO_2 and corresponded with 83

559 significant GO terms associated with stress, signaling, development, and defense. DEGs in
560 cluster 5 were repressed by *Psg*, with greater repression at *e*CO2. The 37 GO terms in cluster
561 5 were largely associated with photosynthesis and response to light.

562 Across all 2,419 DEGs, 74.8% and 83.2% of DEGs responding to *e*CO_2 in *Psg* or mock
563 were also significantly differentially expressed in response to *Psg* at *a*CO_2 and eCO_2,
564 respectively. This confirms that *e*CO_2 impacts the expression of genes involved in pathogen
565 defense responses. This is most obvious in clusters 2 (986 DEGs) and 5 (828 DEGs), where
566 71.1% and 94.3% of DEGs are also significantly differentially expressed in response to *Psg* at
567 *a*CO_2 and 82.3% and 99.5% of DEGs are also significantly *Psg* responsive in *e*CO_2. In summary,
568 the QuantSeq analyses indicate that *e*CO_2 does not cause a reprogramming of responses to
569 *Psg*, but rather it enhances the up- or down-regulation of many genes associated with defense
570 and stress responses and photosynthetic processes.

571 Identification of regulatory elements controlling response to *e*CO_2

572 We next sought to identify the TFs that were differentially expressed in the 2,419 DEGs
573 responding to *e*CO_2 in Figure 5. Across all five clusters, we identified 144 TFs representing 31
574 transcription factor families. Clusters 1-5 contained 7, 43, 27, 19, and 48 unique TFs,
575 respectively (Table S10). Given that many of the GO term descriptions significantly
576 overrepresented in clusters 1 through 5 included the words “response to” or “regulation of”, we
577 were interested in predicting upstream TFs that could also be important in *e*CO_2 responses.
578 Using the DEG list for each cluster as input into PlantRegMap (Tian *et al.*, 2020), we identified
579 1, 44, 18, 13, and 16 significantly overrepresented TF binding sites (TFBS) for clusters 1-5,
580 respectively (Table S11). Interestingly, some predicted TFBS were significant in multiple
581 clusters. In addition, five predicted TFBS were also among our DEGs of interest. We identified
582 the DEG targets corresponding to each overrepresented TFBS (Table S12). In order to assign
583 a possible function to a TF with an overrepresented TFBS, we used the SoyBase GO Term
584 Enrichment Tool (https://www.soybase.org/goslimgraphic_v2/dashboard.php) to identify
585 significantly overrepresented GO terms (corrected $p<0.05$) associated with the corresponding
586 target DEGs (Table S13). Of the 92 significant TFBS predicted, 48 had significantly
587 overrepresented GO terms. Identified GO terms were associated with stress (response to heat,
588 H_2O_2, redox state, phosphate starvation, and light), regulation (cell aging, circadian rhythm,
589 growth rate, proton transport, and transcription), photosynthesis (light reaction, electron

590 transport, and plastid organization), and defense (fatty acid elongation, biosynthesis of
591 anthocyanins, carotenoids, and flavonoids, and negative regulation of defense response to
592 bacterium). Sorting the data in Table S13 revealed multiple TFs were regulating DEGs
593 corresponding to the same GO term. For example, we identified nine significant TFBS
594 associated with photosynthetic electron transport in photosystem I.

595 Given these results, we wanted to examine the TF/TFBS data relative to our DEGs from
596 mock and *Psg*-infected tissues. We plotted the number of target DEGs corresponding to each
597 predicted TFBS (Figure 6a). For almost every predicted TFBS, there were more targets among
598 DEGs from *Psg*-infected tissues than mock-infected tissues, suggesting *Psg* infection resulted
599 in a more robust response to *e*CO_2. To confirm this pattern was not due to errors in predicting
600 TFBS, we also plotted the number of DEGs associated with significantly overrepresented GO
601 terms (Figure 6b; Table S8,S9). For almost every significant GO term, there were more GO
602 terms associated with *Psg*-infected tissues than mock-infected tissues. To better visualize the
603 interaction between TF and TFBS, we used the best Arabidopsis homolog of each TF and TFBS
604 as input into STRING (Szklarczyk *et al.*, 2023). In Figure 6c, TF and TFBS associated with *Psg*-
605 infected tissues are colored shades of teal, while TF and TFBS associated with mock-infected
606 tissues are colored shades of purple. As in 6a and 6b, the TF and TFBS from *Psg*-infected
607 tissues are far more robust, confirming *Psg*-infection enhances responses to *e*CO_2.

608 *e*CO_2 suppresses viral immunity

609 To determine if *e*CO_2 affects virus susceptibility in soybean, we inoculated plants with two virus
610 species, BPMV, a *Comovirus* in the family *Secoviridae* (Sanfaçon *et al.*, 2009), and SMV, a
611 *Potyvirus* in the family *Potyviridae* (Hajimorad *et al.*, 2018). BPMV and SMV caused a greater
612 reduction in soybean growth and shoot dry weight when compared to the mock plants in *e*CO_2
613 than in *a*CO_2 (Figure 7a, S6). Accumulation of BPMV and SMV was higher in the newest fully
614 expanded leaves of infected plants grown at *e*CO_2 compared to those grown at *a*CO_2 at 14 dpi
615 (Figure 7b,c) and to a lesser extent at 21 dpi (Figure S7). Accordingly, the AUDPC was greater
616 for BPMV- and SMV-infected plants grown at *e*CO_2 (Figure 7d,e). We used RT-qPCR to assay
617 expression of soybean homologs of four genes associated with defense responses to viruses:
618 *PR1*, *KTI1*, *AGO1*, and *DCL2*. We found that the overall mean expression of the SA marker
619

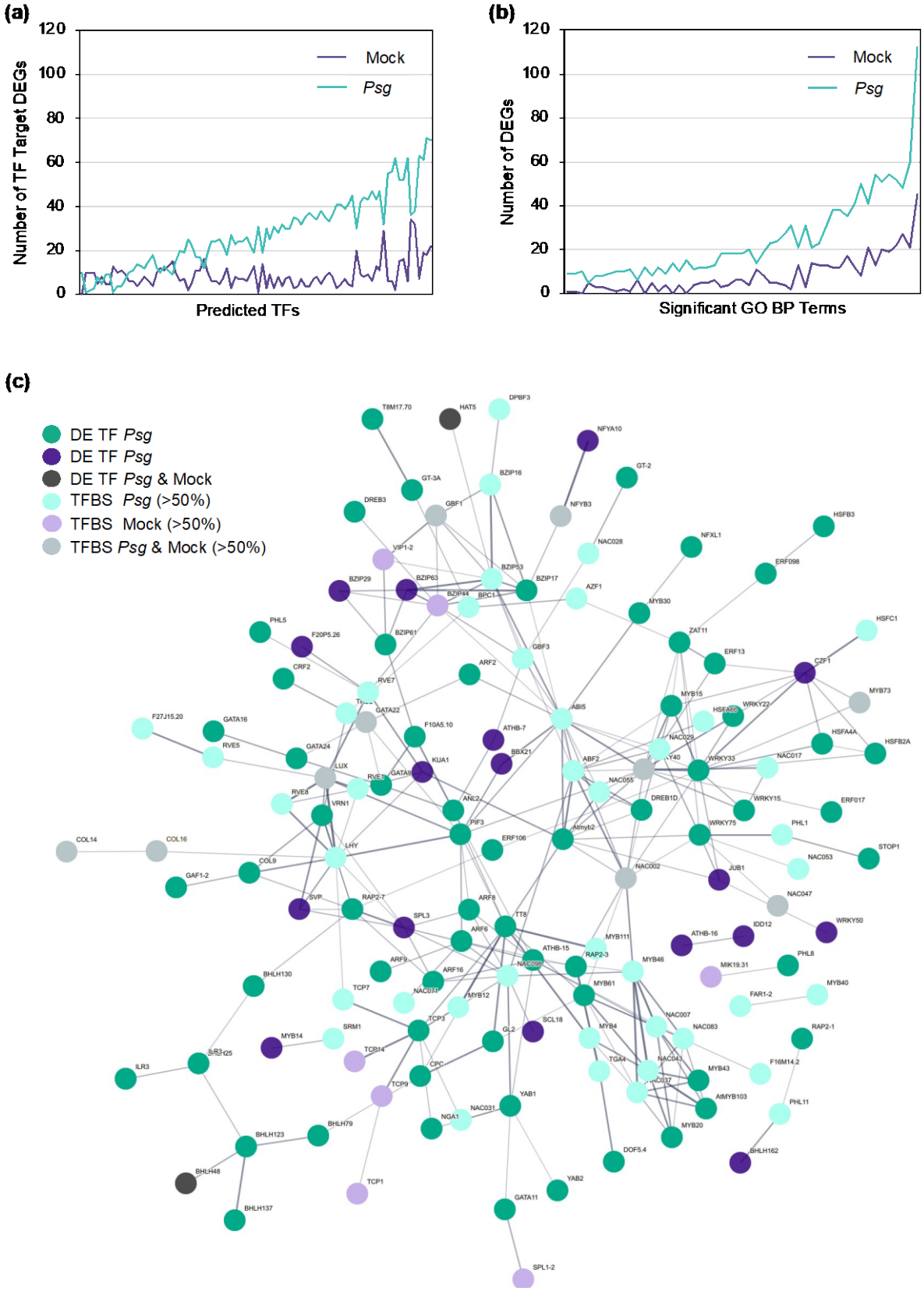

Figure 6. Significantly differentially expressed TFs and over-represented TFBS are more robust in *Psg*-infected tissues responding to eCO_2 than mock infected tissues. PlantRegMap/PlantTFDB v5.0 (Tian *et al.*, 2020) was used to identify significantly differentially expressed TFs and significantly

overrepresented TFBS among the DEG clusters identified in Figure 5 (Supplemental Tables S9-S11). **(a)** Significant TFBS versus predicted number of DEG targets. Overrepresented TFBS and DEGs targets are plotted for every cluster (cluster information not shown), therefore if a TFBS was significant in multiple clusters, it was plotted multiple times but with different DEG targets. **(b)** Significantly overrepresented GO terms (minimum of 10 DEGs per GO term) versus DEG number (Supplemental Table S5). In both panels, DEGs in teal were significant in *Psg* samples and/or DEGs in purple were significant in mock treated samples. **(c)** Best Arabidopsis homologs of TFs and TFBS were input into STRING (Szklarczyk *et al.*, 2023). TFs differentially expressed in response to *e*CO_2 in *Psg*-treated samples, mock-treated samples or both are colored dark teal, dark purple or grey, respectively. TFBS are colored based on the origin of the target DEGs.

gene, *PR1*, was lower at *e*CO_2 when considering both mock and virus-infected plants (Figure 7f). In addition, expression of *PR1* was induced in both BPMV- and SMV-infected plants relative to mock-inoculation under *a*CO_2. However, *PR1* expression in the virus-infected plants was similar to the mock-inoculated plants in *e*CO_2. The expression of *KTI1* was similar under the two CO_2 levels (Figure 7g), and its induction in virus-infected versus mock plants was not significantly different between *a*CO_2 and *e*CO_2, suggesting that JA-mediated defenses against viruses were not affected. We also observed that *AGO1* and *DCL2* accumulated to lower levels in plants grown at *e*CO_2 (Figure 7h,i), suggesting that RNA silencing-based defenses could potentially be compromised (Leonetti *et al.*, 2021; Akbar *et al.*, 2022). These data suggest that the increased susceptibility of soybean to BPMV and SMV under *e*CO_2 may be partially mediated by suppression of SA-related signaling and RNA silencing mechanisms.

Susceptibility to soil-borne filamentous pathogens is altered under elevated CO_2

To determine if *e*CO_2 also impacts susceptibility to soil-borne pathogens, we inoculated soybean with *F. virguliforme*, a hemibiotrophic fungus causing sudden death syndrome (SDS) (O'Donnell *et al.*, 2010), or *P. sylvaticum*, a necrotrophic oomycete causing seed decay and seedling root rot (Rojas *et al.*, 2017). Root and shoot dry weight were decreased to a greater extent in *F. virguliforme*-infected plants grown in *e*CO_2 compared to plants grown under *a*CO_2 at 35 dap (Figure 8a,b, S8). Correspondingly, progression of the foliar symptoms of SDS was greater (Figure 8c) and more severe symptoms developed on the leaves under *e*CO_2 (Figure 8d). Consistent with the increased disease symptoms, *F. virguliforme* was more abundant in the tap roots of plants grown in *e*CO_2 at 35 dap (Figure 8e). To investigate if expression of SA- or JA-

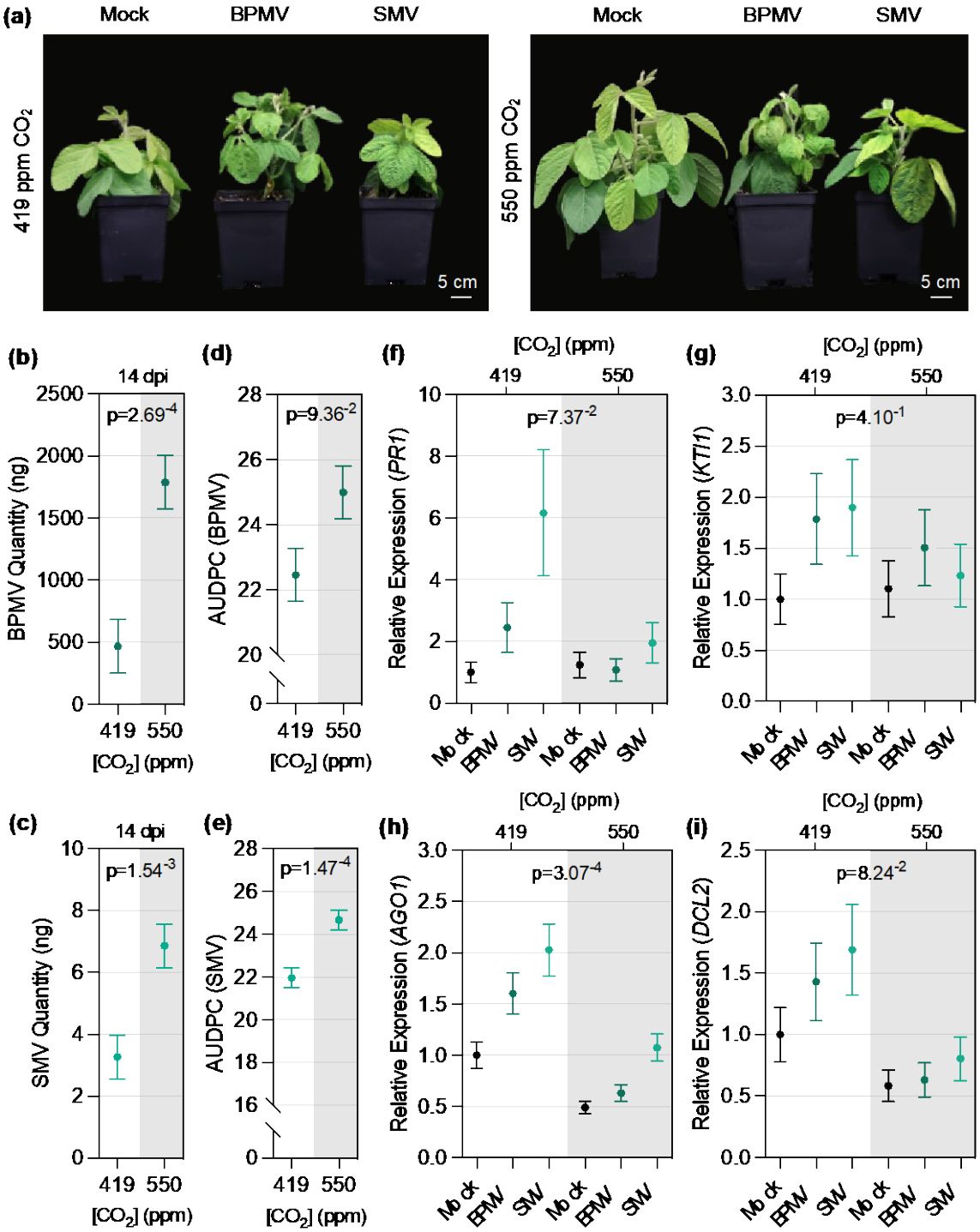

Figure 7. Young soybean plants growing in eCO_2 are more susceptible to BPMV and SMV. (a) Representative photos of soybean growth in response to eCO_2 during infection with BPMV or SMV compared to mock treated control plants. Plants were photographed at 21 days post-inoculation (dpi) **(b)** BPMV and **(c)** SMV quantity at 14 dpi was assessed by RT-qPCR using *Skp1* as a housekeeping gene. Disease progression of **(d)** BPMV and **(e)** SMV calculated as the area under the disease progress curve (AUDPC) over a 35 day time course. Expression of **(f)** *PR1* (SA marker gene) **(g)** *KTI1* (JA marker gene), and RNA silencing-related genes **(h)** *AGO1* and **(i)** *DCL2* in response to BPMV, SMV, or mock treatment was assessed by RT-qPCR analysis relative to the expression of *Skp1*. The newest fully expanded leaves of eight plants were sampled at the indicated time point for each treatment. The three experimental replicates were conducted simultaneously in independent CO_2 controlled chambers using a replicated

670 complete randomized design. Data was graphed as the mean across the three replicates with standard
671 error bars. P-values were computed using F-tests for the main effect of CO_2 from the LMM analysis on
672 the log-transformed relative gene expression data. The following p-values were associated with the log-
673 transformed relative *PR1* expression of virus-infected plants compared to mock-treated plants at *a*CO_2
674 condition: $p(BPMV_{PR1,419})=0.1282$, $p(SMV_{PR1,419})=0.0178$ and at *e*CO_2 condition: $p(BPMV_{PR1,550})=0.7779$,
675 $p(SMV_{PR1,550})=0.3882$. All were calculated based on t-tests for the contrasts between each pathogen and
676 mock at the corresponding CO_2 conditions from the LMM analysis. The following p-values were computed
677 using t-tests from the LMM analysis for the interaction effect between CO_2 condition and pathogen
678 treatment (virus or mock) on log-transformed *KTI1* gene expression: $p(BPMV_{KTI1})=0.6156$ and
679 $p(SMV_{KTI1})=0.3444$.
680
681
682 related defense genes was affected in *e*CO_2, accumulation of *PR1* and *KTI1* mRNA transcripts,
683 respectively, were quantified in soybean roots using RT-qPCR. Expression of neither gene was
684 convincingly altered in response to *F. virguliforme* infection in *e*CO_2 relative to plants grown
685 under *a*CO_2 (Figure 8f, S9). To investigate if *F. virguliforme* growth is affected by [CO_2], we
686 measured the diameter of *F. virguliforme* colonies as they grew on plates for 11 days in *a*CO_2 or
687 *e*CO_2. Fungal growth was similar at the two CO_2 levels (Figure S10), indicating that the greater
688 fungal accumulation in roots and SDS progression observed in soybeans at *e*CO_2 is not caused
689 by increased pathogen replication rate. Together, our data suggest that *e*CO_2 increases
690 susceptibility to *F. virguliforme*, although the underlying molecular mechanisms mediating this
691 altered interaction are unclear.
692
693 Similar to *F. virguliforme*, *P. sylvaticum* caused root rot under both CO_2 treatments (Figure
694 9a), and the root and shoot dry weights of infected plants were more dramatically decreased
695 when compared to the mock treatment in *e*CO_2 relative to *a*CO_2 (Figure 9b, S11). Hyphal growth
696 assays indicated that *P. sylvaticum* grew more quickly in *e*CO_2 than in *a*CO_2 (Figure S12).
697 However, disease index ratings were similar between infected plants grown under both [CO_2]
698 (Figure 9c), which was consistent with the similar *P. sylvaticum* titers observed in roots at 14
699 dap (Figure 9d). Additionally, no difference was observed in *KTI1* expression (Figure 9e), and
700 while the p-value for *PR1* expression was below 0.05, we do not consider it to be significant
701 because of the similar levels of expression in *Pythium*-infected tissue (Figure S13) at 14 dap
702 between the two [CO_2]. Together, our results suggest that *e*CO_2 could have a minor effect on *in*
703 *vitro* growth of *P. sylvaticum*; however, we could not demonstrate that this led to the pathogen
704 being more aggressive in the roots. It is also interesting that while susceptibility to *P. sylvaticum*
705 appears to be unchanged there is a greater loss in root and shoot biomass in plants grown in
706 *e*CO_2.
707

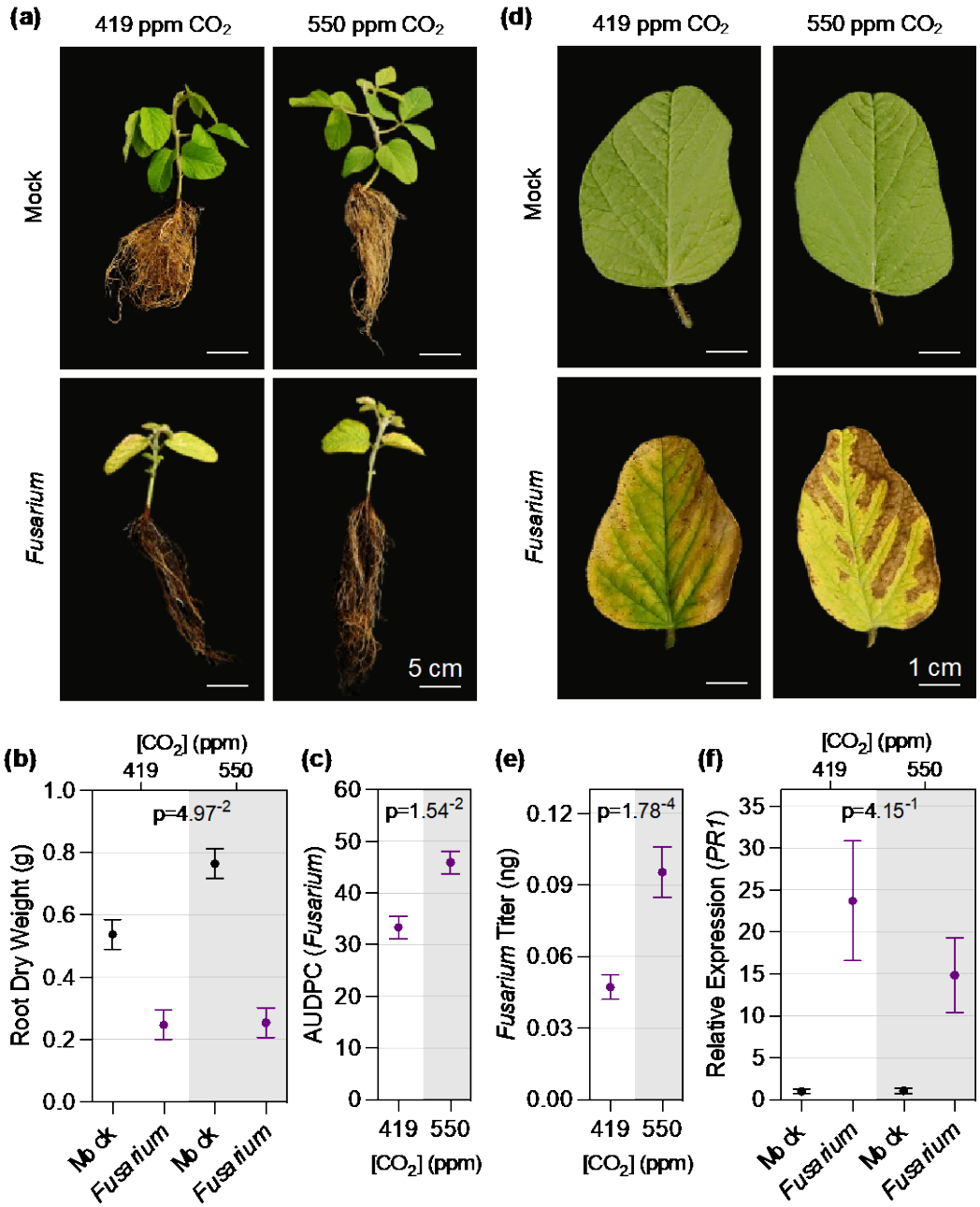

Figure 8. Young soybean plants growing in eCO_2 develop more SDS symptoms and are more susceptible to *F. virguliforme*. (a) Representative photos of soybean plants at 35 days after planting (dap) that were mock treated or germinated in soil infested with *F. virguliforme* and **(b)** associated root dry weight. **(c)** SDS disease progression, assessed as area under the disease progress curve (AUDPC), and **(d)** close-up photos of SDS disease symptoms on unifoliate leaves at 35 dap. **(e)** *F. virguliforme* titer and **(f)** expression of *PR1* (SA marker gene) in soybean roots at 35 dap was assessed by RT-qPCR analysis relative to the *Skp1* housekeeping gene. The three experimental replicates were conducted simultaneously in independent CO_2 controlled chambers using a replicated complete randomized design. Data was graphed as the mean across the three replicates with standard error bars. P-values were computed using F-tests for the main effect of CO_2 on AUDPC and log-transformed titers, and interaction effect between CO_2 and *Fusarium* treatment on root dry weight and log-transformed *PR1* gene expression from the LMM analysis.

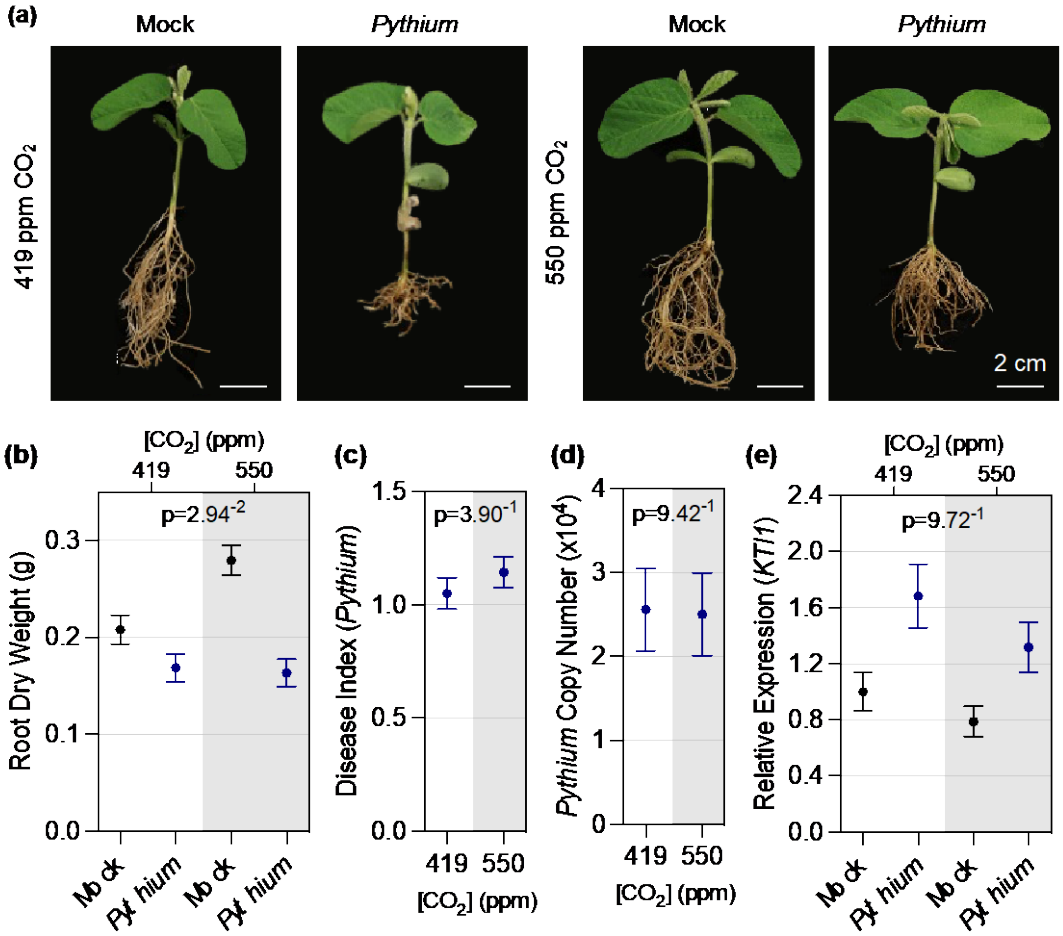

Figure 9. Effects of eCO_2 on *P. sylvaticum* infection in soybean. (a) Representative photos of soybean plants at 21 days after planting (dap) that were mock treated or germinated in soil infested with *P. sylvaticum* and **(b)** associated root dry weight. **(c)** *P. sylvaticum* disease index measured 14 dap and **(d)** *P. sylvaticum* copy number in roots determined by RT-qPCR analysis at 21 dap. **(e)** *KTI1* (JA marker gene) expression in response to mock treatment or *P. sylvaticum* infection assessed by RT-qPCR analysis. Gene expression was assessed relative to the *Skp1* housekeeping gene. The three experimental replicates were conducted simultaneously in independent CO_2 controlled chambers using a replicated complete randomized design. Data was graphed as the mean across the three replicates with standard error bars. P-values were computed using F-tests for the main effect of CO_2 on AUDPC and *Pythium* copy number, and interaction effect between CO_2 and *Pythium* treatment on root dry weight and log-transformed *KTI1* expression from the LMM analysis.

Discussion

Climate change is impacting agriculture by affecting crop quality and yield (Pareek *et al.*, 2020; Rezaei *et al.*, 2023), and CO_2 is considered to be the primary driver of climate change because of its abundance and longevity in the atmosphere. Given the central role of CO_2 in plant biology, there are many ways it can influence plant physiology that can potentially impact interactions with pathogenic microbes (Bazinet *et al.*, 2022). While some themes are beginning to emerge,

742 it remains challenging to predict the response of a given plant to a given pathogen under *e*CO_2.
743 Here, we selected a diverse panel of phytopathogens to assess if and how soybean-microbe
744 interactions are impacted by *e*CO_2. Our results demonstrate that the CO_2 levels expected within
745 the next three decades (Jaggard *et al.*, 2010) have significant impacts on soybean immunity.
746 The effects of *e*CO_2 on disease varied across the different pathogen types with enhanced
747 resistance to bacterial blight caused by *Psg*, increased susceptibility to BPMV, SMV, and *F.*
748 *virguliforme*, and little apparent effect on susceptibility to *P. sylvaticum*.

749 Extensive research from SoyFACE experiments has demonstrated that under favorable
750 environmental conditions, *e*CO_2 (550 ppm CO_2) has the potential to benefit soybean growth and
751 yield (Long *et al.*, 2006; Ainsworth & Long, 2021). To determine if our *e*CO_2 experiments in
752 controlled environment chambers could approximate the effects on soybean growth and
753 physiology that have been observed in SoyFACE experiments, we conducted baseline
754 physiological and gene expression analyses. In line with field results, we observed that leaf
755 photosynthetic rate and plant biomass increased, whereas stomatal conductance, density, and
756 aperture decreased (Figure 1). Interestingly, we found that expression of some photosynthesis-
757 related genes, such as *Rubisco small subunit 1B* (*RbcS1B*), decreased under eCO_2, which
758 seems contradictory to the enhanced photosynthesis. However, others have shown that mRNA
759 expression of *RbcS* and other photosynthesis-related genes can be down-regulated as non-
760 structural sugars accumulate and plants begin to acclimate to *e*CO_2 (Cheng *et al.*, 1998;
761 Thompson *et al.*, 2017). The combined results from physiology and baseline gene expression
762 analyses indicated that the soybean plants were performing as expected in *e*CO_2 under our
763 growth conditions and support the idea that their responses to pathogens would be authentic.

764 Although the impacts of *e*CO_2 on soybean physiology are well-established, its effects on
765 disease are limited to one study that investigated the incidence and severity of three naturally
766 occurring diseases caused by the fungal pathogens *F. virguliforme* (SDS) and *Septoria glycines*
767 (brown spot) and the oomycete pathogen *Peronospora manshurica* (downy mildew) over three
768 years in SoyFACE (Eastburn *et al.*, 2010). *e*CO_2 did not affect SDS incidence or severity, but
769 the severity of brown spot disease increased, while the severity of downy mildew decreased.
770 The incidence of brown spot and downy mildew were not affected. The results from this study
771 are consistent with the idea that diseases caused by necrotrophic pathogens may be typically
772 enhanced under *e*CO_2, whereas diseases caused by biotrophic and hemibiotrophic pathogens
773 may be suppressed in C3 plants (Bazinet *et al.*, 2022). This study showed that future
774 atmospheric CO_2 levels have the potential to positively or negatively impact soybean diseases

775 that occur in the field, but it was limited by the pathogens that were present, variable
776 environmental conditions, and unknown levels of inoculum. Our goal was to extend these
777 findings under controlled environmental conditions to determine how *e*CO_2 differentially affects
778 responses to distinct types of pathogens and to establish a foundation to understand the
779 complex and dynamic signaling events that influence soybean-pathogen interactions in
780 response to *e*CO_2.

781 The effects of [CO_2] on bacterial infection have not been investigated previously in
782 soybean, however, several independent studies have indicated that for the hemibiotrophic
783 pathogen *Pto*DC3000, *e*CO_2 enhances resistance in tomato (Li *et al.*, 2015; Zhang *et al.*, 2015;
784 Hu *et al.*, 2021) and mostly increases susceptibility in Arabidopsis (Zhou *et al.*, 2017, 2019).
785 Arabidopsis does not become more susceptible to all pathogens, as it is more resistant to
786 infection with the necrotrophic pathogen *B. cinerea* at *e*CO_2 (Zhou *et al.*, 2019). In our work, we
787 observed enhanced resistance in compatible interactions between *Psg* and soybean under
788 *e*CO_2, and to a lesser extent, during incompatible interactions with *Pto*DC3000 and *Pto*DC3000
789 *hrcC*$^-$ (Figure 3A). Taken together, it is evident that bacterial immunity is altered under *e*CO_2 in
790 C3 plants in a pathosystem-specific manner. Notably, changes in environmental conditions,
791 nutrient availability, and other growth conditions have been shown to alter the direction of these
792 responses (Bazinet *et al.*, 2022).

793 Phytohormones and stomatal immunity play pivotal roles in altering defense responses
794 to bacteria under *e*CO_2 in Arabidopsis and tomato. For example, in tomato, enhanced resistance
795 to *Pto*DC3000 was associated with *e*CO_2-induced stomatal closure (Li *et al.*, 2015) and higher
796 SA biosynthesis (Li *et al.*, 2015; Zhang *et al.*, 2015). In Arabidopsis, increased susceptibility to
797 *Pto*DC3000 was associated with reduced ABA levels, causing changes in stomatal dynamics
798 favoring bacterial infection (Zhou *et al.*, 2017), and shifts in SA/JA antagonism toward JA-
799 mediated immunity against necrotrophic pathogens (Zhou *et al.*, 2019). In response to *Psg*
800 infection, we observed a 1.7-fold increase in SA accumulation and no notable change in JA
801 levels (Figure S4). However, this slight increase in SA seems unlikely to provide the level of
802 resistance against *Psg* observed under *e*CO_2 based on previous work showing that free SA was
803 increased by 7-10 fold in soybean plants exhibiting SA-dependent, constitutive defense
804 responses (Liu *et al.*, 2011). We hypothesize that enhanced bacterial resistance is likely
805 conferred by a combination of physiological, metabolic, and molecular responses that together
806 limit bacterial infection under *e*CO_2. Indeed, we observed an upregulation of MAMP-triggered
807 immune responses in soybeans at *e*CO_2 including flg22-induced oxidative species production

808 (Figure 4b) and flg22-induced MAPK activation (Figure 4c). We additionally observed reduced
809 stomatal density (Figure 1c) and a constitutive decrease in stomatal aperture (Figure 1d), which
810 is likely to limit the entry of bacterial species.

811 Our transcriptomic analysis also indicates that *e*CO_2 has direct impacts on soybean
812 defense. *e*CO_2 caused an over-representation of DEGs associated with defense responses
813 (Figure 2, Table S5), even in the absence of pathogen challenge. Most notable was altered
814 expression of genes associated with JA signaling and response to JA, including decreased
815 expression of *Jasmonate Zim Domain* (*JAZ*)-encoding genes, which repress jasmonate
816 signaling, and *MYC2* orthologs, known as the master regulators of jasmonate signaling (Johnson
817 *et al.*, 2023). Although we did not observe higher baseline JA levels under *e*CO_2 in our
818 metabolomics analysis (Figure S4), down-regulation of these genes suggests that JA-mediated
819 responses may be altered in soybean plants growing in *e*CO_2. This finding is consistent with
820 prior work demonstrating that various insects prefer to feed on and cause more damage to plants
821 grown in *e*CO_2 (DeLucia *et al.*, 2008; Johnson *et al.*, 2020), which has been attributed at least
822 in part to compromised JA-mediated defenses (Zavala *et al.*, 2008). We also found no evidence
823 for constitutive up-regulation of SA-mediated defenses under *e*CO_2, because there were no
824 pathogenesis-related genes among our DEGs and SA levels were not different from plants
825 grown in *a*CO_2. However, we did find that some genes that positively regulate basal defense
826 responses were upregulated, suggesting that some immune responses might be primed in
827 soybean under these conditions. The effects of *e*CO_2 on DEGs was even more pronounced
828 following *Psg* infection (Figure 5; Table S8). Similar DEGs were identified at *a*CO_2 and *e*CO_2 in
829 response to *Psg* infection, however the amplitude of these responses were significantly more
830 up- or down-regulated, depending on the gene, in response to *e*CO_2 (Table S8). This is in line
831 with the higher *Psg*- and flg22-elicited defense gene expression and basal defense responses
832 under *e*CO_2.

833 The effects of *e*CO_2 on virus susceptibility has been studied in various other C3 plants,
834 most of which have reported increased resistance to viral pathogens associated with a
835 constitutive overproduction of SA (Fu *et al.*, 2010; Trębicki *et al.*, 2016) or upregulation of RNA
836 silencing genes that are critical for viral defense (Guo *et al.*, 2020). As discussed above, we did
837 not observe a constitutive stimulation of SA levels or SA-based defenses in our experimental
838 system, and interestingly, we found that expression of two genes potentially involved in anti-viral
839 RNA silencing was decreased (Figure 7h,i). In line with our molecular analyses, soybean plants
840 were more susceptible to BPMV and SMV in *e*CO_2. Increased susceptibility could be partially

841 explained by reduced induction of SA-based defenses, as indicated by reduced *PR1* gene
842 expression in BPMV- and SMV-treated plants in *e*CO_2 (Figure 7f). It is also possible that changes
843 in RNA silencing components are responsible for increased susceptibility, as we observed a
844 reduction in both *AGO1* (Figure 7h) and *DCL2* (Figure 7i) expression in virus-infected soybean
845 at *e*CO_2. Our results suggest that both SA-mediated defense and RNA silencing are
846 compromised in response to BPMV and SMV infection in soybean. An interesting avenue to
847 pursue in the future would be to test if there is a link between the apparent down-regulation of
848 SA-mediated defenses and anti-viral RNA silencing.

849 Many viruses, including BPMV and SMV, are transmitted by an insect vector in nature.
850 Importantly, many of the studies indicating that plants are less susceptible to viruses under *e*CO_2
851 have used aphids as a vector for viral delivery. Thus, we do not know if the presence of bean
852 leaf beetle (BPMV) or aphid (SMV) may influence the outcome of the interaction. Furthermore,
853 the behavior of insect vectors or other factors may be influenced by *e*CO_2 in ways that could
854 affect dissemination of the viruses. For example, the larger canopy size associated with
855 increased photosynthetic rates in soybean are expected to cause a higher dispersion rate,
856 increasing disease incidence and severity in the field (Amari *et al.*, 2021), pointing to viruses as
857 potential pathogens of concern under predicted future climatic conditions. It will be interesting to
858 study the tri-trophic interactions in the future from mechanistic and epidemiological perspectives,
859 and perhaps including other climate change-associated gasses such as ozone, which retards
860 SMV infection in soybean (Bilgin *et al.*, 2008).

861 *e*CO_2 has been shown to have various effects on diseases caused by fungi and
862 oomycetes (filamentous pathogens). Fungal pathogens are of particular concern under predicted
863 future climatic conditions as it will allow their dispersal into more Northern latitudes as a
864 consequence of higher temperatures and predicted changes in annual precipitation and humidity
865 levels (Nnadi & Carter, 2021). While various studies have investigated the effect of *e*CO_2 on
866 filamentous pathogens (Smith & Luna, 2023), relatively few have examined soil-borne
867 pathogens. Elevated CO_2 (800 ppm) had no effect on infections caused by *Rhizoctonia solani*
868 or *F. oxysporum* in Arabidopsis plants (Zhou *et al.*, 2019). Tomato plants grown in 700 ppm CO_2
869 were more tolerant to root rot caused by *Phytophthora infestans* (Jwa & Walling, 2001). Growth
870 of *P. infestans* was not directly affected by [CO_2] and the increased resistance of tomato plants
871 could not be associated with changes in expression of marker genes associated with SA-, ABA,
872 or JA-based defenses. In FACE experiments involving natural infections, *e*CO_2 led to higher
873 incidence of sheath blight (*Rhizoctonia solani*) on rice (Kobayashi *et al.*, 2006), but SDS (*F.*

874 *virguliforme*) in soybean was not affected (Eastburn *et al.*, 2010). Interestingly, the increased
875 incidence of rice sheath blight was only observed in plots that also received input of high nitrogen
876 fertilizer. These previous studies show that responses of plants to filamentous soil-borne
877 pathogens can be affected by *e*CO_2, but they can be highly influenced by environmental factors
878 and do not necessarily correlate with the expected defense-related signaling events.

879 Our data indicate that soybean plants are more susceptible to *F. virguliforme* under *e*CO_2
880 but had no notable change in *P. sylvaticum* infection. Surprisingly, we observed a greater loss
881 in root and shoot dry weight in response to *P. sylvaticum* even though visual disease scores
882 were similar, and similar quantities of *P. sylvaticum* DNA were observed in the roots of plants
883 grown at *e*CO_2 and *a*CO_2. We only observed a modest reduction in *PR1* expression following *F.*
884 *virguliforme* treatment under *e*CO_2, and there was no change in expression of the *KTI1* JA
885 marker gene. These gene expression results are similar to what has previously been observed
886 in tomato with increased susceptibility showing no correlation with concomitant changes in
887 expression of defense pathway marker genes (Jwa & Walling, 2001). Various other factors have
888 been linked to *F. virguliforme* resistance, which we did not assess in this study, including the
889 production of phytoalexins and changes in root exudates, both of which can be affected by *e*CO_2
890 (Vaughan *et al.*, 2014; Usyskin-Tonne *et al.*, 2020). Experiments at FACE facilities have
891 demonstrated dramatic changes in the soil microbial rhizosphere and endosphere (Rosado-
892 Porto *et al.*, 2022; Gao *et al.*, 2022), which could also impact the composition of phytopathogenic
893 fungi in the surrounding soil and cause changes in soybean-pathogen interactions. One could
894 also expect that changes in root architecture and growth could benefit or curtail infection by soil
895 pathogens. Our data indicate that disease losses due to soil-borne filamentous pathogens can
896 be exacerbated in soybean grown in *e*CO_2, and there is much more to learn about the underlying
897 mechanisms.

898 In conclusion, we have demonstrated that soybean basal defense responses and gene
899 expression are altered under *e*CO_2, differentially regulating susceptibility to bacterial, viral,
900 fungal, and oomycete pathogens. Comprehensive analysis of bacterially-elicited responses has
901 given us a strong foundation to investigate which genes are regulating defense to bacteria under
902 *e*CO_2 and how the corresponding signaling pathways are regulated. In our experiments, we
903 assessed the effect of [CO_2] on pathogen growth, however, we did not investigate how pathogen
904 virulence or evolution affects soybean-pathogen interactions under these conditions. In our
905 study, we focused on the impact of one factor, *e*CO_2, on soybean physiology and disease
906 susceptibility. However, *e*CO_2 is not the only environmental factor to consider when predicting

907 the outcome of future climatic conditions on plant health. Increases in temperature, changes in
908 water and nutrient availability, soil pH, photoperiod, and severe weather events are also
909 expected to affect disease susceptibility (Saijo & Loo, 2020). For example, higher temperatures
910 have almost uniformly been associated with higher disease susceptibility to bacterial pathogens
911 in Arabidopsis (Cohen & Leach, 2020). Understanding how combined stresses, in the context of
912 future atmospheric CO_2 levels that are likely to occur, affect defense signaling and disease
913 development is a critical question that needs to be investigated further to develop new strategies
914 to mitigate crop losses due to threats imposed by climate change.
915

916 Acknowledgments

917 We acknowledge the ISU DNA Facility, Office of Biotechnology, Iowa State University, Ames IA
918 for providing analytical instrumentation and technical expertise. We acknowledge the Iowa State
919 University W.M. Keck Metabolomics Research Laboratory (RRID:SCR_017911) for providing
920 analytical instrumentation. We thank Dr. Gwyn Beattie (ISU) for providing us with the *Pto*DC3000
921 *hrcC*- strain, Dr. Leanor Leandro and Vijitha K. Silva (ISU) for SDS inoculum and inoculation
922 protocols, and Dr. Alison E. Robertson and Clarice L. Schmidt (ISU) for *P. sylvaticum* inoculum
923 and guidance with infection experiments. This work was supported in part by the Iowa Soybean
924 Research Center, the ISU Plant Sciences Institute, USDA NIFA Hatch Project 4308, the ISU
925 College of Agriculture and Life Sciences and by USDA-ARS projects 5030-21220-007-000D
926 (Leveraging Crop Genetic Diversity and Genomics to Improve Biotic and Abiotic Stress
927 Tolerance in Soybean) and 0500-00093-001-00-D (SCINet). Ekkachai Khwanbua is supported
928 by an Anandamahidol fellowship from the government of Thailand. Mention of trade names or
929 commercial products in this publication is solely for the purpose of providing specific information
930 and does not imply recommendation or endorsement by the USDA. USDA-ARS is an equal
931 opportunity employer and provider.

932 Competing Interests

933 The authors declare that they have no competing interests.

Author Contributions

EK, MB, ASC, and KH performed the experiments. MB, EK, and SAW conceived of the experiments. MWB performed the metabolomics analysis. YQ and PL performed statistical analysis using the linear mixed models. MAG performed the QuantSeq data analysis. MB, EK, MAG, and SAW wrote the manuscript with contributions from all authors.

Data Availability

The RNA-seq reads for QuantSeq dataset 1 and dataset 2 were deposited in NCBI under BioProject PRJNA1017882 and PRJNA1017884, respectively. The authors declare that any additional supporting data for this work can be found in the manuscript, its supplementary materials, or obtained directly from the corresponding author upon request.

References

Aguilar E, Allende L, Del Toro FJ, Chung B-N, Canto T, Tenllado F. **2015**. Effects of Elevated CO_2 and Temperature on Pathogenicity Determinants and Virulence of Potato virus X/Potyvirus-Associated Synergism. *Molecular Plant-Microbe Interactions: MPMI* **28**: 1364–1373.

Ahammed GJ, Li X. **2022**. Elevated carbon dioxide-induced regulation of ethylene in plants. *Environmental and Experimental Botany* **202**: 105025.

Ainsworth EA, Long SP. **2021**. 30 years of free-air carbon dioxide enrichment (FACE): What have we learned about future crop productivity and its potential for adaptation? *Global Change Biology* **27**: 27–49.

Akbar S, Wei Y, Zhang M-Q. **2022**. RNA Interference: Promising Approach to Combat Plant Viruses. *International Journal of Molecular Sciences* **2323** (10): 5312**.**

Amari K, Huang C, Heinlein M. **2021**. Potential Impact of Global Warming on Virus Propagation in Infected Plants and Agricultural Productivity. *Frontiers in Plant Science* **12**: 649768.

Aspray EK, Mies TA, McGrath JA, Montes CM, Dalsing B, Puthuval KK, Whetten A, Herriott J, Li S, Bernacchi CJ, *et al.* 2023. Two decades of fumigation data from the Soybean Free Air Concentration Enrichment facility. *Scientific Data* **10**: 226.

Morgan M, Pagès H, Obenchain V, and Hayden N. 2021. Rsamtools: Binary alignment (BAM), FASTA, variant call (BCF), and tabix file import. Available at: https://bioconductor.org/packages/Rsamtools.

Bao Y, Zarecor S, Shah D, Tuel T, Campbell DA, Chapman AVE, Imberti D, Kiekhaefer D, Imberti H, Lübberstedt T, *et al.* 2019. Assessing plant performance in the Enviratron. *Plant Methods* **15**: 117.

Bazinet Q, Tang L, Bede JC. **2022**. Impact of Future Elevated Carbon Dioxide on C Plant Resistance to Biotic Stresses. *Molecular Plant-Microbe Interactions: MPMI* **35**: 527–539.

Bebber DP, Ramotowski MAT, Gurr SJ. **2013**. Crop pests and pathogens move polewards in a warming world. *Nature Climate Change* **3**: 985–988.

Beyer SF, Bel PS, Flors V, Schultheiss H, Conrath U, Langenbach CJG. **2021**. Disclosure of salicylic acid and jasmonic acid-responsive genes provides a molecular tool for deciphering stress responses in soybean. *Scientific Reports* **11**: 20600.

Bilgin DD, Aldea M, O'Neill BF, Benitez M, Li M, Clough SJ, DeLucia EH. **2008**. Elevated ozone alters soybean-virus interaction. *Molecular Plant-Microbe Interactions* **21**: 1297–1308.

Bolger AM, Lohse M, Usadel B. **2014**. Trimmomatic: a flexible trimmer for Illumina sequence data. *Bioinformatics* **30**: 2114–2120.

979 **Bredow M, Sementchoukova I, Siegel K, Monaghan J**. **2019**. Pattern-Triggered Oxidative
980 Burst and Seedling Growth Inhibition Assays in Arabidopsis thaliana. *Journal of Visualized*
981 *Experiments: JoVE* **147**: e59437.

982 **Broberg M, Högy P, Pleijel H**. **2017**. CO_2-Induced Changes in Wheat Grain Composition:
983 Meta-Analysis and Response Functions. *Agronomy* **7**: 32.

984 **Brooks DM, Hernández-Guzmán G, Kloek AP, Alarcón-Chaidez F, Sreedharan A,**
985 **Rangaswamy V, Peñaloza-Vázquez A, Bender CL, Kunkel BN**. **2004**. Identification and
986 characterization of a well-defined series of coronatine biosynthetic mutants of Pseudomonas
987 syringae pv. tomato DC3000. *Molecular Plant-Microbe Interactions* **17**: 162–174.

988 **Budde IP, Ullrich MS**. **2000**. Interactions of Pseudomonas syringae pv. glycinea with host and
989 nonhost plants in relation to temperature and phytotoxin synthesis. *Molecular Plant-Microbe*
990 *Interactions* **13**: 951–961.

991 **Casteel CL, O'Neill BF, Zavala JA, Bilgin DD, Berenbaum MR, Delucia EH**. **2008**.
992 Transcriptional profiling reveals elevated CO_2 and elevated O_3 alter resistance of soybean
993 (Glycine max) to Japanese beetles (Popillia japonica). *Plant, Cell & Environment* **31**: 419–434.

994 **Ceulemans R, VAN Praet L, Jiang XN**. **1995**. Effects of CO_2 enrichment, leaf position and
995 clone on stomatal index and epidermal cell density in poplar (Populus). *New Phytologist* **131**:
996 99–107.

997 **Chakraborty S**. **2013**. Migrate or evolve: options for plant pathogens under climate change.
998 *Global Change Biology* **19**: 1985–2000.

999 **Cheng SH, Moore B, Seemann JR**. **1998**. Effects of short- and long-term elevated CO_2 on the
1000 expression of ribulose-1,5-bisphosphate carboxylase/oxygenase genes and carbohydrate
1001 accumulation in leaves of Arabidopsis thaliana (L.) Heynh. *Plant Physiology* **116**: 715–723.

1002 **Christian N, Espino Basurto B, Toussaint A, Xu X, Ainsworth EA, Busby PE, Heath KD**.
1003 **2021**. Elevated carbon dioxide reduces a common soybean leaf endophyte. *Global Change*
1004 *Biology* **27**: 4154–4168.

1005 **Cohen & Leach**. **2020**. High temperature-induced plant disease susceptibility: more than the
1006 sum of its parts. *Current Opinion in Plant Biology* **56**: 235–241.

1007 **DeFalco TA, Zipfel C**. **2021**. Molecular mechanisms of early plant pattern-triggered immune
1008 signaling. *Molecular Cell* **81**: 4346.

1009 **DeLucia EH, Casteel CL, Nabity PD, O'Neill BF**. **2008**. Insects take a bigger bite out of
1010 plants in a warmer, higher carbon dioxide world. *Proceedings of the National Academy of*
1011 *Sciences* **105**: 1781–1782.

1012 **Dermody O, O'Neill BF, Zangerl AR, Berenbaum MR, DeLucia EH**. **2008**. Effects of
1013 elevated CO_2 and O_3 on leaf damage and insect abundance in a soybean agroecosystem.
1014 *Arthropod-Plant Interactions* **2**: 125–135.

1015 **Dobin A, Davis CA, Schlesinger F, Drenkow J, Zaleski C, Jha S, Batut P, Chaisson M,**
1016 **Gingeras TR**. **2013**. STAR: ultrafast universal RNA-seq aligner. *Bioinformatics* **29**: 15–21.

1017 **Dusenge ME, Duarte AG, Way DA**. **2019**. Plant carbon metabolism and climate change:
1018 elevated CO_2 and temperature impacts on photosynthesis, photorespiration and respiration.
1019 *New Phytologist* **221**: 32–49.

1020 **Dziuda DM**. **2010**. *Data Mining for Genomics and Proteomics: Analysis of Gene and Protein*
1021 *Expression Data*. New York: John Wiley & Sons.

1022 **Eastburn DM, Degennaro MM, Delucia EH, Dermody O, Mcelrone AJ**. **2010**. Elevated
1023 atmospheric carbon dioxide and ozone alter soybean diseases at SoyFACE. *Global Change*
1024 *Biology* **16**: 320–330.

1025 **Foyer CH, Noctor G**. **2020**. Redox Homeostasis and Signaling in a Higher CO_2 World. *Annual*
1026 *Review of Plant Biology* **71**: 157–182.

1027 **Fu X, Ye L, Kang LE, Ge F**. **2010**. Elevated CO_2 shifts the focus of tobacco plant defences
1028 from cucumber mosaic virus to the green peach aphid. *Plant, Cell & Environment* **33**: 2056–
1029 2064.

1030 **Gao K, Mao Z, Meng E, Li J, Liu X, Zhang Y, Zhang L, Wang G, Liu Y**. **2022**. Effects of
1031 elevated CO_2 and warming on the root-associated microbiota in an agricultural ecosystem.
1032 *Environmental Microbiology* **24**: 6252–6266.

1033 **Gonçalves HV, Oki Y, Bordignon L, Ferreira MC, Dos Santos JE Jr, Tameirão LBS,**
1034 **Santos FR, Kalapothakis E, Fernandes GW**. **2021**. Endophytic fungus diversity in soybean
1035 plants submitted to conditions of elevated atmospheric CO_2 and temperature. *Canadian*
1036 *Journal of Microbiology* **67**: 290–300.

1037 **Grulke NE**. **2011**. The nexus of host and pathogen phenology: understanding the disease
1038 triangle with climate change. *New Phytologist* **189**: 8–11.

1039 **Guo H, Ge P, Tong J, Zhang Y, Peng X, Zhao Z, Ge F, Sun Y**. **2020**. Elevated Carbon
1040 Dioxide Levels Decreases Cucumber Mosaic Virus Accumulation in Correlation with Greater
1041 Accumulation of rgs-CaM, an Inhibitor of a Viral Suppressor of RNAi. *Plants* **10**(1): 59.

1042 **Gupta K, Lalit M, Biswas A, Sanada CD, Greene C, Hukari K, Maulik U, Bandyopadhyay**
1043 **S, Ramalingam N, Ahuja G, *et al.* 2021**. Modeling expression ranks for noise-tolerant
1044 differential expression analysis of scRNA-seq data. *Genome Research* **31**: 689–697.

1045 **Hajimorad MR, Domier LL, Tolin SA, Whitham SA, Saghai Maroof MA**. **2018**. Soybean
1046 mosaic virus: a successful potyvirus with a wide distribution but restricted natural host range.
1047 *Molecular Plant Pathology* **19**: 1563–1579.

1048 **Huang L, Ren Q, Sun Y, Ye L, Cao H, Ge F**. **2012**. Lower incidence and severity of tomato
1049 virus in elevated CO_2 is accompanied by modulated plant induced defence in tomato. *Plant*
1050 *Biology* **14**: 905–913.

1051 **Hu Z, Ma Q, Foyer CH, Lei C, Choi HW, Zheng C, Li J, Zuo J, Mao Z, Mei Y, *et al.* 2021**.
1052 High CO_2- and pathogen-driven expression of the carbonic anhydrase βCA3 confers basal
1053 immunity in tomato. *New Phytologist* **229**: 2827–2843.

1054 **Jaggard KW, Qi A, Ober ES**. **2010**. Possible changes to arable crop yields by 2050.

1055 *Philosophical Transactions of the Royal Society of London. Series B, Biological Sciences* **365**:
1056 2835–2851.

1057 **Jiye A, Trygg J, Gullberg J, Johansson AI, Jonsson P, Antti H, Marklund SL, Moritz T**.
1058 **2005**. Extraction and GC/MS analysis of the human blood plasma metabolome. *Analytical*
1059 *Chemistry* **77**: 8086–8094.

1060 **Johnson LYD, Major IT, Chen Y, Yang C, Vanegas-Cano LJ, Howe GA**. **2023**.
1061 Diversification of JAZ-MYC signaling function in immune metabolism. *New Phytologist* **239**:
1062 2277–2291.

1063 **Johnson SN, Waterman JM, Hall CR**. **2020**. Increased insect herbivore performance under
1064 elevated CO_2 is associated with lower plant defence signalling and minimal declines in
1065 nutritional quality. *Scientific Reports* **10**: 14553.

1066 **Jwa N-S, Walling LL**. **2001**. Influence of elevated CO_2 concentration on disease development
1067 in tomato. *New Phytologist* **149**: 509–518.

1068 **Kobayashi T, Ishiguro K, Nakajima T, Kim HY, Okada M, Kobayashi K**. **2006**. Effects of
1069 Elevated Atmospheric CO_2 Concentration on the Infection of Rice Blast and Sheath Blight.
1070 *Phytopathology* **96**: 425–431.

1071 **Koek MM, Muilwijk B, van der Werf MJ, Hankemeier T**. **2006**. Microbial metabolomics with
1072 gas chromatography/mass spectrometry. *Analytical Chemistry* **78**: 1272–1281.

1073 **Kojima M, Kamada-Nobusada T, Komatsu H, Takei K, Kuroha T, Mizutani M, Ashikari M,**
1074 **Ueguchi-Tanaka M, Matsuoka M, Suzuki K, *et al.* 2009**. Highly sensitive and high-throughput
1075 analysis of plant hormones using MS-probe modification and liquid chromatography-tandem
1076 mass spectrometry: an application for hormone profiling in Oryza sativa. *Plant & Cell*
1077 *Physiology* **50**: 1201–1214.

1078 **Kojima M, Sakakibara H**. **2012**. Highly sensitive high-throughput profiling of six
1079 phytohormones using MS-probe modification and liquid chromatography-tandem mass
1080 spectrometry. *Methods in Molecular Biology* **918**: 151–164.

1081 **Kumudini S**. **2010**. Soybean growth and development. *The soybean: botany, production and*
1082 *uses*: 48–73. epublication: CABI.

1083 **Lake JA, Wade RN**. **2009**. Plant-pathogen interactions and elevated CO_2: morphological
1084 changes in favour of pathogens. *Journal of Experimental Botany* **60**: 3123–3131.

1085 **Lawrence M, Gentleman R, Carey V**. **2009**. rtracklayer: an R package for interfacing with
1086 genome browsers. *Bioinformatics* **25**(14): 1841-1842.

1087 **Leonetti P, Stuttmann J, Pantaleo V**. **2021**. Regulation of plant antiviral defense genes via
1088 host RNA-silencing mechanisms. *Virology Journal* **18**: 194.

1089 **Li C, Gu X, Wu Z, Qin T, Guo L, Wang T, Zhang L, Jiang G**. **2021**. Assessing the effects of
1090 elevated ozone on physiology, growth, yield and quality of soybean in the past 40 years: A
1091 meta-analysis. *Ecotoxicology and Environmental Safety* **208**: 111644.

1092 **Li H, Handsaker B, Wysoker A, Fennell T, Ruan J, Homer N, Marth G, Abecasis G, Durbin**
1093 **R, 1000 Genome Project Data Processing Subgroup**. **2009**. The Sequence Alignment/Map
1094 format and SAMtools. *Bioinformatics* **25**: 2078–2079.

1095 **Lindeberg M, Cunnac S, Collmer A**. **2009**. The evolution of Pseudomonas syringae host
1096 specificity and type III effector repertoires. *Molecular Plant Pathology* **10**: 767–775.

1097 **Li X, Sun Z, Shao S, Zhang S, Ahammed GJ, Zhang G, Jiang Y, Zhou J, Xia X, Zhou Y, *et***
1098 ***al.* 2015**. Tomato-Pseudomonas syringae interactions under elevated CO_2 concentration: the
1099 role of stomata. *Journal of Experimental Botany* **66**: 307–316.

1100 **Liu J-Z, Horstman HD, Braun E, Graham MA, Zhang C, Navarre D, Qiu W-L, Lee Y,**
1101 **Nettleton D, Hill JH, *et al.* 2011**. Soybean homologs of MPK4 negatively regulate defense
1102 responses and positively regulate growth and development. *Plant Physiology* **157**: 1363–1378.

1103 **Liu X, Sun Y, Kørner CJ, Du X, Vollmer ME, Pajerowska-Mukhtar KM**. **2015**. Bacterial Leaf
1104 Infiltration Assay for Fine Characterization of Plant Defense Responses using the Arabidopsis
1105 thaliana-Pseudomonas syringae Pathosystem. *Journal of Visualized Experiments: JoVE* **104**:
1106 53364.

1107 **Long SP, Ainsworth EA, Leakey ADB, Nösberger J, Ort DR**. **2006**. Food for thought: lower-
1108 than-expected crop yield stimulation with rising CO_2 concentrations. *Science* **312**: 1918–1921.

1109 **Matros A, Amme S, Kettig B, Buck-Sorlin GH, Sonnewald U, Mock H-P**. **2006**. Growth at
1110 elevated CO_2 concentrations leads to modified profiles of secondary metabolites in tobacco cv.
1111 Samsun and to increased resistance against infection with potato virus Y. *Plant, Cell &*
1112 *Environment* **29**: 126–137.

1113 **Matthiesen RL, Ahmad AA, Robertson AE**. **2016**. Temperature Affects Aggressiveness and
1114 Fungicide Sensitivity of Four Pythium spp. that Cause Soybean and Corn Damping Off in Iowa.
1115 *Plant Disease* **100**: 583–591.

1116 **McCarthy DJ, Chen Y, Smyth GK**. **2012**. Differential expression analysis of multifactor RNA-
1117 Seq experiments with respect to biological variation. *Nucleic Acids Research* **40**: 4288–4297.

1118 **Mhamdi A, Noctor G**. **2016**. High CO_2 Primes Plant Biotic Stress Defences through Redox-
1119 Linked Pathways. *Plant Physiology* **172**: 929–942.

1120 **Murphy AM, Zhou T, Carr JP**. **2020**. An update on salicylic acid biosynthesis, its induction
1121 and potential exploitation by plant viruses. *Current Opinion in Virology* **42**: 8–17.

1122 **Murtagh F**. **1985**. *Multidimensional Clustering Algorithms*. Heidelberg: Physica.

1123 **Myers SS, Zanobetti A, Kloog I, Huybers P, Leakey ADB, Bloom AJ, Carlisle E, Dietterich**
1124 **LH, Fitzgerald G, Hasegawa T, *et al.* 2014**. Increasing CO_2 threatens human nutrition. *Nature*
1125 **510**: 139–142.

1126 **Ngou BPM, Ding P, Jones JDG**. **2022**. Thirty years of resistance: Zig-zag through the plant
1127 immune system. *The Plant Cell* **34**: 1447–1478.

1128 **Nnadi NE, Carter DA**. **2021**. Climate change and the emergence of fungal pathogens. *PLoS*

1129 *Pathogens* **17**: e1009503.

1130 **Noctor G, Mhamdi A**. **2017**. Climate Change, CO_2, and Defense: The Metabolic, Redox, and
1131 Signaling Perspectives. *Trends in Plant Science* **22**: 857–870.

1132 **Ode PJ, Johnson SN, Moore BD**. **2014**. Atmospheric change and induced plant secondary
1133 metabolites - are we reshaping the building blocks of multi-trophic interactions? *Current*
1134 *Opinion in Insect Science* **5**: 57–65.

1135 **O'Donnell K, Sink S, Scandiani MM, Luque A, Colletto A, Biasoli M, Lenzi L, Salas G,**
1136 **González V, Ploper LD, *et al.* 2010**. Soybean sudden death syndrome species diversity within
1137 North and South America revealed by multilocus genotyping. *Phytopathology* **100**: 58–71.

1138 **O'Neill BF, Zangerl AR, Dermody O, Bilgin DD, Casteel CL, Zavala JA, DeLucia EH,**
1139 **Berenbaum MR**. **2010**. Impact of elevated levels of atmospheric CO_2 and herbivory on
1140 flavonoids of soybean (Glycine max Linnaeus). *Journal of Chemical Ecology* **36**: 35–45.

1141 **Pangga IB, Chakraborty S, Yates D**. **2007**. Canopy Size and Induced Resistance in
1142 Stylosanthes scabra Determine Anthracnose Severity at High CO_2. *Phytopathology* **94**: 221-
1143 227.

1144 **Pan C, Zhang H, Ma Q, Fan F, Fu R, Ahammed GJ, Yu J, Shi K**. **2019**. Role of ethylene
1145 biosynthesis and signaling in elevated CO_2-induced heat stress response in tomato. *Planta*
1146 **250**: 563–572.

1147 **Pareek A, Dhankher OP, Foyer CH**. **2020**. Mitigating the impact of climate change on plant
1148 productivity and ecosystem sustainability. *Journal of Experimental Botany* **71**: 451–456.

1149 **Paulo PD, Pereira EJG, Oliveira EE, Fereres A, Garzo E**. **2020.** CO_2 concentration on
1150 *Bemisia tabaci* MEAM1 feeding on *Bt* soybean plants. *Journal of Applied Entomology* **144**:
1151 941–951.

1152 **Petre B, Louet C, Lintz J, Duplessis S**. **2022**. 2000-2019: Twenty Years of Highly Influential
1153 Publications in Molecular Plant Immunity. *Molecular Plant-Microbe Interactions* **35**: 748–754.

1154 **Pinto H, Sharwood RE, Tissue DT, Ghannoum O**. **2014**. Photosynthesis of C3, C3–C4, and
1155 C4 grasses at glacial CO_2. *Journal of Experimental Botany* **65**: 3669–3681.

1156 **Prom LK, Venette JR**. **1997**. Races of Pseudomonas syringae pv. glycinea on Commercial
1157 Soybean in Eastern North Dakota. *Plant Disease* **81**: 541–544.

1158 **Pruitt RN, Locci F, Wanke F, Zhang L, Saile SC, Joe A, Karelina D, Hua C, Fröhlich K,**
1159 **Wan W-L, *et al.* 2021**. The EDS1–PAD4–ADR1 node mediates Arabidopsis pattern-triggered
1160 immunity. *Nature* **598**: 495–499.

1161 **Raza and Bebber**. **2022**. Climate change and plant pathogens. *Current Opinion in*
1162 *Microbiology* **70**: 102233.

1163 **Rezaei EE, Webber H, Asseng S, Boote K, Durand JL, Ewert F, Martre P, MacCarthy DS**.
1164 **2023**. Climate change impacts on crop yields. *Nature Reviews Earth & Environment* **4**: 831–
1165 846.

1166 **Robinson MD, McCarthy DJ, Smyth GK**. **2010**. edgeR: a Bioconductor package for
1167 differential expression analysis of digital gene expression data. *Bioinformatics* **26**: 139–140.

1168 **Robinson MD, Smyth GK**. **2007**. Moderated statistical tests for assessing differences in tag
1169 abundance. *Bioinformatics* **23**: 2881–2887.

1170 **Rogers SO, Bendich AJ**. **1994**. Extraction of total cellular DNA from plants, algae and fungi.
1171 In: Gelvin SB, Schilperoort RA, eds. Plant Molecular Biology Manual. Dordrecht: Springer
1172 Netherlands, 183–190.

1173 **Rojas JA, Jacobs JL, Napieralski S, Karaj B, Bradley CA, Chase T, Esker PD, Giesler LJ,**
1174 **Jardine DJ, Malvick DK, *et al.* 2017**. Oomycete Species Associated with Soybean Seedlings
1175 in North America-Part II: Diversity and Ecology in Relation to Environmental and Edaphic
1176 Factors. *Phytopathology* **107**: 293–304.

1177 **Rosado-Porto D, Ratering S, Cardinale M, Maisinger C, Moser G, Deppe M, Müller C,**
1178 **Schnell S**. **2022**. Elevated Atmospheric CO_2 Modifies Mostly the Metabolic Active
1179 Rhizosphere Soil Microbiome in the Giessen FACE Experiment. *Microbial Ecology* **83**: 619-634.

1180 **Roth MG, Noel ZA, Wang J, Warner F, Byrne AM, Chilvers MI**. **2019**. Predicting Soybean
1181 Yield and Sudden Death Syndrome Development Using At-Planting Risk Factors.
1182 *Phytopathology* **109**: 1710–1719.

1183 **Ryalls JMW, Moore BD, Riegler M, Gherlenda AN, Johnson SN**. **2015**. Amino acid-
1184 mediated impacts of elevated carbon dioxide and simulated root herbivory on aphids are
1185 neutralized by increased air temperatures. *Journal of Experimental Botany* **66**: 613–623.

1186 **Saijo Y, Loo EP-I**. **2020**. Plant immunity in signal integration between biotic and abiotic stress
1187 responses. *New Phytologist* **225**: 87–104.

1188 **Sanfaçon H, Wellink J, Le Gall O, Karasev A, van der Vlugt R, Wetzel T**. **2009**.
1189 Secoviridae: a proposed family of plant viruses within the order Picornavirales that combines
1190 the families Sequiviridae and Comoviridae, the unassigned genera Cheravirus and
1191 Sadwavirus, and the proposed genus Torradovirus. *Archives of Virology* **154**: 899–907.

1192 **Savary S, Willocquet L, Pethybridge SJ, Esker P, McRoberts N, Nelson A**. **2019**. The
1193 global burden of pathogens and pests on major food crops. *Nature Ecology & Evolution* **3**:
1194 430–439.

1195 **Schmutz J, Cannon SB, Schlueter J, Ma J, Mitros T, Nelson W, Hyten DL, Song Q,**
1196 **Thelen JJ, Cheng J, *et al.* 2010**. Genome sequence of the palaeopolyploid soybean. *Nature*
1197 **463**: 178–183.

1198 **de Sena Brandine G, Smith AD**. **2019**. Falco: high-speed FastQC emulation for quality
1199 control of sequencing data. *F1000Research* **8**: 1874.

1200 **Simko I, Piepho H-P**. **2012**. The area under the disease progress stairs: calculation,
1201 advantage, and application. *Phytopathology* **102**: 381–389.

1202 **Singh BK, Delgado-Baquerizo M, Egidi E, Guirado E, Leach JE, Liu H, Trivedi P**. **2023**.
1203 Climate change impacts on plant pathogens, food security and paths forward. *Nature Reviews*

1204 *Microbiology* **21**: 640–656.

1205 **Smith F, Luna E**. **2023**. Elevated atmospheric carbon dioxide and plant immunity to fungal
1206 pathogens: do the risks outweigh the benefits? *Biochemical Journal* **480**: 1791–1804.

1207 **Sultana SN, Park H, Choi SH, Jo H, Song JT, Lee J-D, Kang YJ**. **2021**. Optimizing the
1208 Experimental Method for Stomata-Profiling Automation of Soybean Leaves Based on Deep
1209 Learning. *Plants* **10**: 2714.

1210 **Sun Y, Guo H, Ge F**. **2016**. Plant-Aphid Interactions Under Elevated CO_2: Some Cues from
1211 Aphid Feeding Behavior. *Frontiers in Plant Science* **7**: 502.

1212 **Szklarczyk D, Kirsch R, Koutrouli M, Nastou K, Mehryary F, Hachilif R, Gable AL, Fang T,**
1213 **Doncheva NT, Pyysalo S, *et al.* 2023**. The STRING database in 2023: protein-protein
1214 association networks and functional enrichment analyses for any sequenced genome of
1215 interest. *Nucleic Acids Research* **51**: D638-D646.

1216 **Taub DR, Miller B, Allen H**. **2008**. Effects of elevated CO_2 on the protein concentration of
1217 food crops: a meta-analysis. *Global Change Biology* **14**: 565–575.

1218 **Thompson M, Gamage D, Hirotsu N, Martin A, Seneweera S**. **2017**. Effects of Elevated
1219 Carbon Dioxide on Photosynthesis and Carbon Partitioning: A Perspective on Root Sugar
1220 Sensing and Hormonal Crosstalk. *Frontiers in Physiology* **8**: 578.

1221 **Tian F, Yang D-C, Meng Y-Q, Jin J, Gao G**. **2020**. PlantRegMap: charting functional
1222 regulatory maps in plants. *Nucleic Acids Research* **48**: D1104–D1113.

1223 **Timm S, Bauwe H**. **2013**. The variety of photorespiratory phenotypes - employing the current
1224 status for future research directions on photorespiration. *Plant Biology* **15**: 737–747.

1225 **Trębicki P, Vandegeer RK, Bosque-Pérez NA, Powell KS, Dader B, Freeman AJ, Yen AL,**
1226 **Fitzgerald GJ, Luck JE**. **2016**. Virus infection mediates the effects of elevated CO_2 on plants
1227 and vectors. *Scientific Reports* **6**: 22785.

1228 **Usyskin-Tonne A, Hadar Y, Yermiyahu U, Minz D**. **2020**. Elevated CO_2 and nitrate levels
1229 increase wheat root-associated bacterial abundance and impact rhizosphere microbial
1230 community composition and function. *The ISME Journal* **15**: 1073–1084.

1231 **Vaughan MM, Huffaker A, Schmelz EA, Dafoe NJ, Christensen S, Sims J, Martins VF,**
1232 **Swerbilow J, Romero M, Alborn HT, *et al.* 2014**. Effects of elevated [CO_2] on maize defence
1233 against mycotoxigenic Fusarium verticillioides. *Plant, Cell & Environment* **37**: 2691–2706.

1234 **Velásquez AC, Castroverde CDM, He SY**. **2018**. Plant-Pathogen Warfare under Changing
1235 Climate Conditions. *Current Biology* **28**: R619–R634.

1236 **Vlot AC, Dempsey DA, Klessig DF**. **2009**. Salicylic Acid, a multifaceted hormone to combat
1237 disease. *Annual Review of Phytopathology* **47**: 177–206.

1238 **Voss I, Sunil B, Scheibe R, Raghavendra AS**. **2013**. Emerging concept for the role of
1239 photorespiration as an important part of abiotic stress response. *Plant Biology* **15**: 713–722.

1240 **Wang J, Grubb LE, Wang J, Liang X, Li L, Gao C, Ma M, Feng F, Li M, Li L, *et al.* 2018**. A
1241 Regulatory Module Controlling Homeostasis of a Plant Immune Kinase. *Molecular Cell* **69**:
1242 493–504.

1243 **Whalen MC, Innes RW, Bent AF, Staskawicz BJ**. **1991**. Identification of Pseudomonas
1244 syringae pathogens of Arabidopsis and a bacterial locus determining avirulence on both
1245 Arabidopsis and soybean. *The Plant Cell* **3**: 49–59.

1246 **Whitham SA, Qi M, Innes RW, Ma W, Lopes-Caitar V, Hewezi T**. **2016**. Molecular Soybean-
1247 Pathogen Interactions. *Annual Review of Phytopathology* **54**: 443–468.

1248 **Wickham H**. **2009**. *ggplot2: Elegant Graphics for Data Analysis*. New York: Springer Science
1249 & Business Media.

1250 **Xu H-Y, Zhang C, Li Z-C, Wang Z-R, Jiang X-X, Shi Y-F, Tian S-N, Braun E, Mei Y, Qiu W-**
1251 **L, *et al.* 2018**. The MAPK Kinase Kinase GmMEKK1 Regulates Cell Death and Defense
1252 Responses. *Plant Physiology* **178**: 907–922.

1253 **Yeh Y-H, Panzeri D, Kadota Y, Huang Y-C, Huang P-Y, Tao C-N, Roux M, Chien H-C, Chin**
1254 **T-C, Chu P-W, *et al.* 2016**. The Arabidopsis Malectin-Like/LRR-RLK IOS1 Is Critical for BAK1-
1255 Dependent and BAK1-Independent Pattern-Triggered Immunity. *The Plant Cell* **28**: 1701–
1256 1721.

1257 **Yu Z, Li Y, Wang G, Liu J, Liu J, Liu X, Herbert SJ, Jin J**. **2016**. Effectiveness of elevated
1258 CO_2 mediating bacterial communities in the soybean rhizosphere depends on genotypes.
1259 *Agriculture, Ecosystems & Environment* **231**: 229–232.

1260 **Zavala JA, Casteel CL, Delucia EH, Berenbaum MR**. **2008**. Anthropogenic increase in
1261 carbon dioxide compromises plant defense against invasive insects. *Proceedings of the*
1262 *National Academy of Sciences of the United States of America* **105**: 5129–5133.

1263 **Zhang S, Li X, Sun Z, Shao S, Hu L, Ye M, Zhou Y, Xia X, Yu J, Shi K**. **2015**. Antagonism
1264 between phytohormone signalling underlies the variation in disease susceptibility of tomato
1265 plants under elevated CO_2. *Journal of Experimental Botany* **66**: 1951–1963.

1266 **Zhang BQ, Yang XB**. **2000**. Pathogenicity of Pythium Populations from Corn-Soybean
1267 Rotation Fields. *Plant Disease* **84**: 94–99.

1268 **Zhou X, Lindsay H, Robinson MD**. **2014**. Robustly detecting differential expression in RNA
1269 sequencing data using observation weights. *Nucleic Acids Research* **42**: e91.

1270 **Zhou Y, Van Leeuwen SK, Pieterse CMJ, Bakker PAH, Van Wees SCM**. **2019**. Effect of
1271 atmospheric CO_2 on plant defense against leaf and root pathogens of Arabidopsis. *European*
1272 *Journal of Plant Pathology* **154**: 31–42.

1273 **Zhou Y, Vroegop-Vos I, Schuurink RC, Pieterse CMJ, Van Wees SCM**. **2017**. Atmospheric
1274 CO2 Alters Resistance of Arabidopsis to Pseudomonas syringae by Affecting Abscisic Acid
1275 Accumulation and Stomatal Responsiveness to Coronatine. *Frontiers in Plant Science* **8:** 700.

1276 **Zhu C, Hu Y, Mao H, Li S, Li F, Zhao C, Luo L, Liu W, Yuan X**. **2021**. A Deep Learning-
1277 Based Method for Automatic Assessment of Stomatal Index in Wheat Microscopic Images of

1278 Leaf Epidermis. *Frontiers in Plant Science* **12**: 716784.

1279

Supporting Information

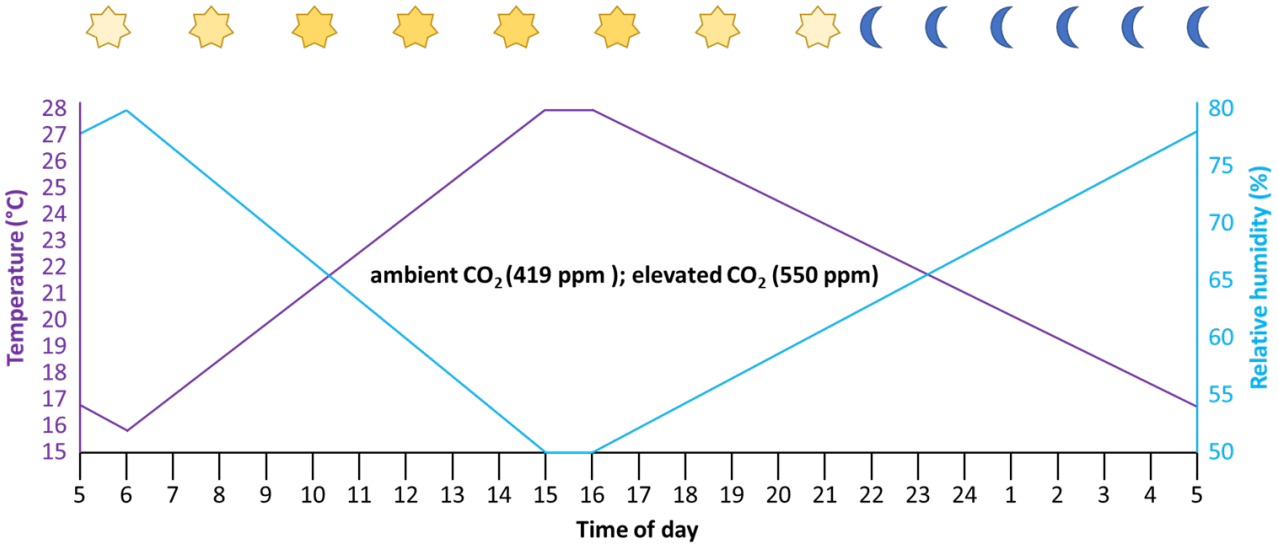

Figure S1. Schematic representation of growth chamber conditions. Schematic representation of Enviratron growth chamber conditions. All chambers were set to the same conditions, except that CO_2 was 419 ppm in chambers set to ambient (*a*CO_2) conditions and CO_2 was 550 ppm in elevated (*e*CO_2) conditions. Lights were on at 5:38 am (05:38) and off at 8:52 pm (22:52) (sunrise and sunset times represent June 15 in central Iowa), minimum temperature was 15.6 °C at 6 am (06:00) with ramping to 27.6 °C maximum temperature from 3:00 – 4:00 pm (15:00 – 16:00). The relative humidity was ramped between 80% at 6:00 am (0:600) to the minimum of 50% at 3:00 – 4:00 pm (15:00-16:00).

1293

1294

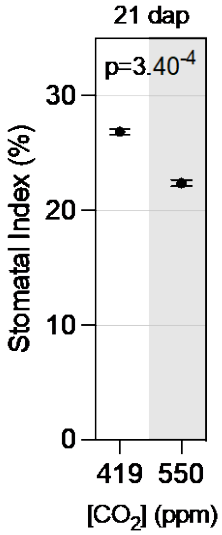

1295

1296

1297 **Figure S2. Stomatal index on the abaxial leaf surface of soybean.** Stomatal index measurements
1298 were performed as described in materials and methods. Three replicates were carried out simultaneously
1299 in independent CO_2 control chambers, using 5 plants per treatment for each CO_2 concentration. Stomata
1300 were counted in three randomly selected fields of view per leaf. Data points represent the mean value
1301 across the three replicates, and error bars represent the standard error. P-value was computed based
1302 on an F-test for the main effect of CO_2 in linear mixed effect model analysis.

1303

1304

1305

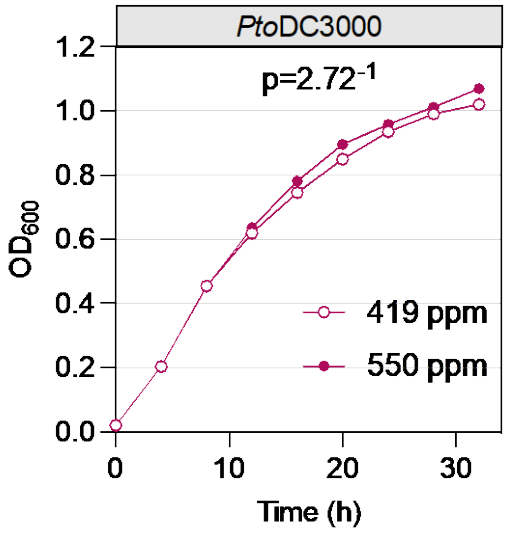

1306

1307

1308 **Figure S3. Effect of elevated CO_2 on growth rate of *Pseudomonas syringae* pv. *tomato* DC3000**
1309 **(*Pst*DC3000).** Bacterial cultures were grown in LB broth without antibiotics for 32 h and OD_{600} was
1310 measured every four hours using a portable spectrophotometer. Two experimental replicates were
1311 conducted simultaneously, for each CO_2 concentration, in independent CO_2 chambers. Data points
1312 represent the average OD_{600} between the two chambers. P-value was computed based on an F-test for
1313 the interaction of CO_2 and time in linear mixed effect model analysis using data after 4 hours due to
1314 unequal variance.
1315

1316

1317

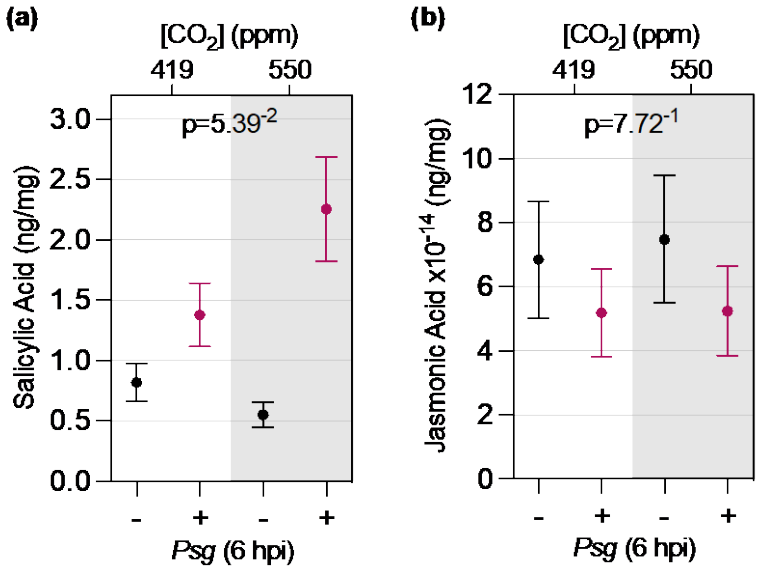

1318

1319

1320 **Figure S4. Accumulation of SA and JA at 6 h post-inoculation with *Pseudomonas syringae* pv.**
1321 ***glycinea* (*Psg*) in *a*CO_2 and *e*CO_2. (a)** SA and **(b)** JA levels were quantified using non-targeted and
1322 targeted metabolomics analysis, respectively, as described in methods and materials. Experiments were
1323 conducted independently, three times, using 8 plants per treatment for each CO_2 concentration. Data
1324 points represent the mean value across the three replicates and error bars represent the standard error.
1325 P-value was computed based on an F-test for the interaction of CO_2 and *Psg* treatment in linear mixed
1326 effect model analysis on log-transformed data.

1327

1328

1329

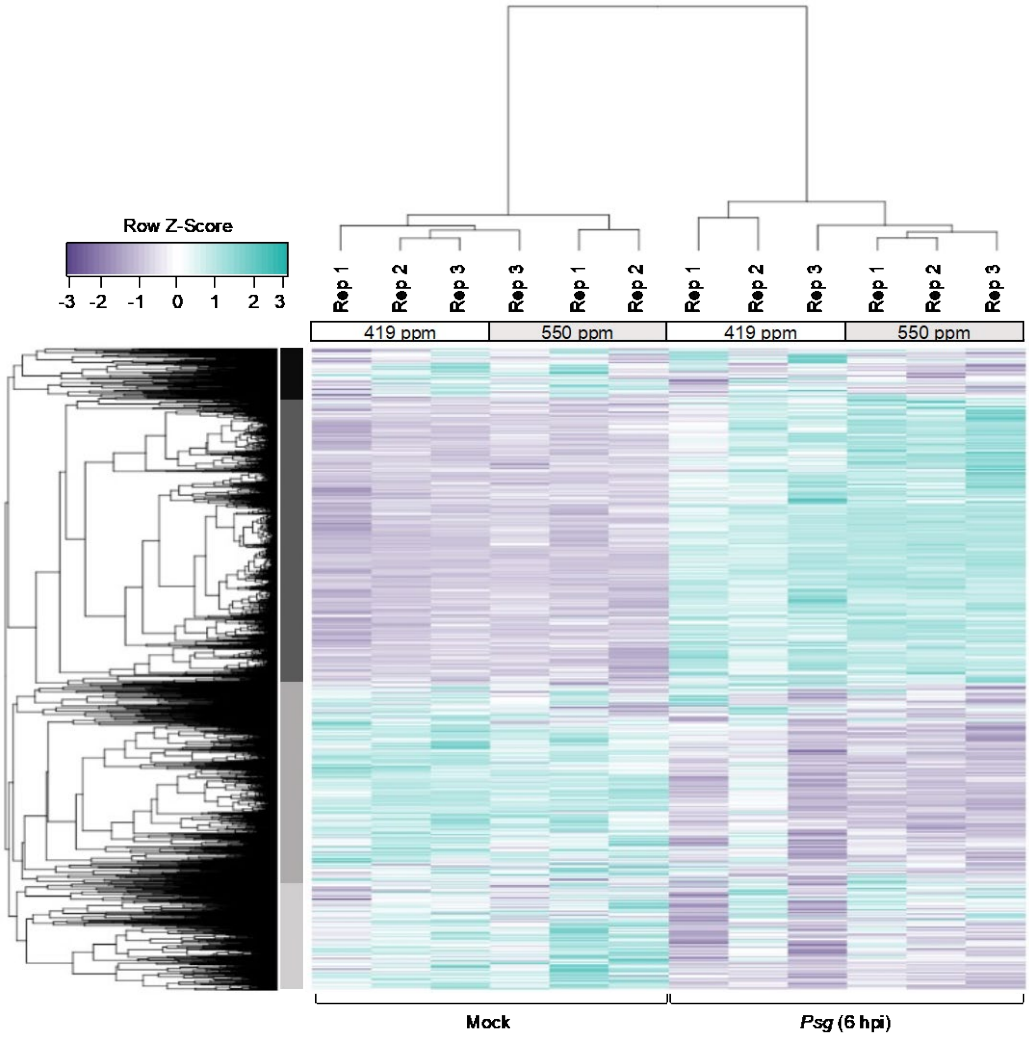

1330

1331

1332 **Figure S5. Hierarchical clustering of 21,822 DEGs (FDR < 0.01) responding to *Pseudomonas***
1333 ***syringae* pv. *glycinea* (*Psg*) at 6 h post-inoculation in plants grown in *e*CO_2 (550 ppm) or *a*CO_2 (419**
1334 **ppm) conditions.** The full list of DEGs is provided in Table S7. Samples for QuantSeq analysis were
1335 taken from the unifoliate leaves of 14-day old plants at 6 h post-inoculation with mock treatment or *Psg*.
1336 The three independent replicates were conducted using eight plants per CO_2 treatment. Rep indicates
1337 independent biological replicates. Row Z-scores were used for hierarchical clustering of DEGs, based on
1338 expression across samples and replicates. Purple indicates expression values below the row mean and
1339 teal indicates expression values above the row mean. Four different expression clusters were identified.
1340 These are indicated by differently shaded gray boxes to the left of the heat map.

1341

1342

1343

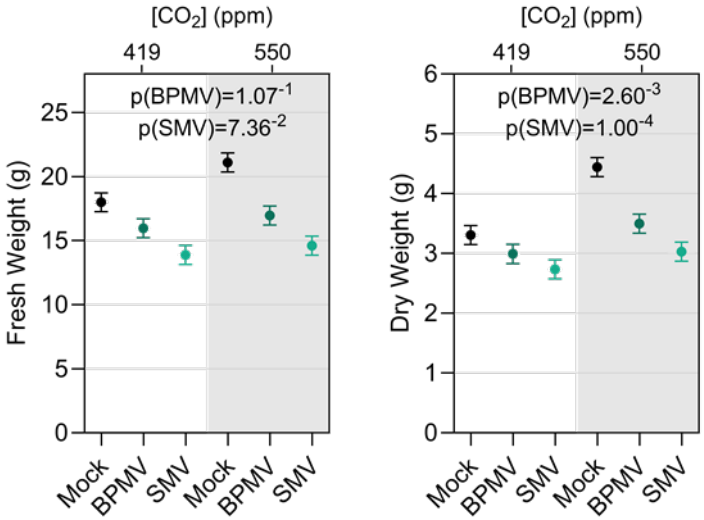

1344

1345

1346 **Figure S6. Effect of elevated CO_2 on the shoot fresh weight and shoot dry weight of soybean**
1347 **plants infected with bean pod mottle virus (BPMV) and soybean mosaic virus (SMV). (a)** Fresh
1348 weight and **(b)** dry weight of soybean plants at 21 days post-inoculation with BPMV, SMV, or mock
1349 treatment. Three experiments were conducted simultaneously in independent CO_2 control chambers,
1350 using 8 plants per treatment for each CO_2 concentration according to a replicated complete design. Data
1351 points represent the mean value across the three replicates and error bars represent the standard error.
1352 P-values were computed based on t-tests for comparing the difference between virus and Mock under
1353 eCO_2 with that under aCO_2 in linear mixed effect model analysis.

1354

1355

1356

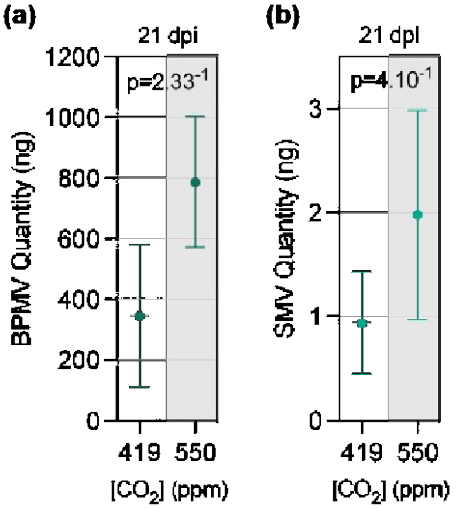

1357

1358

1359 **Figure S7. Bean pod mottle virus (BPMV) and soybean mosaic virus (SMV) accumulation at 21**
1360 **days post-inoculation in soybean plants growing in *a*CO_2 and *e*CO_2. (a)** BPMV and **(b)** SMV quantity
1361 was determined by RT-qPCR using multiplexed probes for BPMV or SMV and *Skp1* as an internal
1362 reference control. Samples were taken from the newest fullest expanded leaf. Three experiments were
1363 conducted simultaneously in independent CO_2 chambers, using 8 plants per infection treatment for each
1364 CO_2 concentration according to a replicated complete block design. Data points and bars represent mean
1365 group values and standard error across the three replicates. P-value for BPMV was computed based on
1366 an F-test for the main effect of CO_2 in linear mixed effect model analysis. P-value for SMV was computed
1367 based on an F-test for the main effect of CO_2 in linear mixed effect model analysis on log-transformed
1368 data.

1369

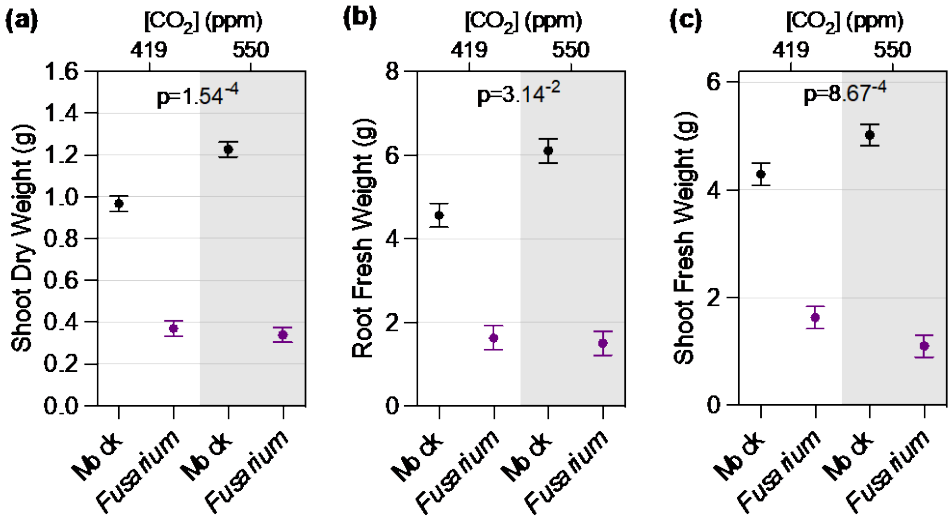

Figure S8. Effects of eCO_2 on root and shoot biomass of soybean plants infected with *Fusarium virguliforme*. (a) Shoot dry weight, **(b)** root fresh weight and **(c)** shoot fresh weight at 35 days after germination in soil infested with *F. virguliforme* or mock infested. The three replicate experiments were conducted simultaneously in independent CO_2 control chambers using 6 plants per treatment for each CO_2 condition according to a replicated complete block design. Data points represent mean values with standard error across the three replicates. P-values were computed based on F-tests for the interaction effect between CO_2 and *Fusarium* treatment in linear mixed effect model analysis.

1382

1383

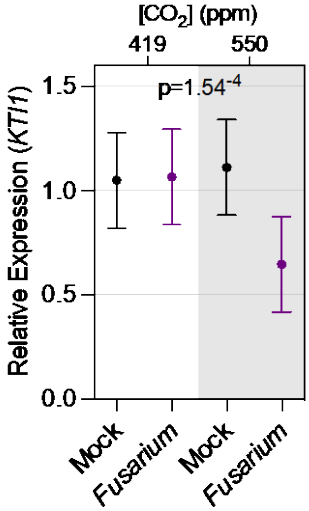

1384

1385

1386 **Figure S9. Expression of the JA marker gene, *KTI1*, in roots of plants infected with *Fusarium***
1387 ***virguliforme* in *a*CO_2 and *e*CO_2.** RT-qPCR analysis was conducted on RNA extracted from root tissue
1388 using gene-specific primers for the JA marker gene *KTI1* with *Skp1* as an internal reference control.
1389 Experiments were conducted using 6 plants per treatment for each CO_2 concentration. Triplicate
1390 experiments were conducted simultaneously in independent CO_2 chambers. Data points and bars
1391 represent mean values and standard error across the three replicates. P-value was computed based on
1392 an F-test for the interaction effect between CO_2 and *Fusarium* treatment in linear mixed effect model
1393 analysis.

1394

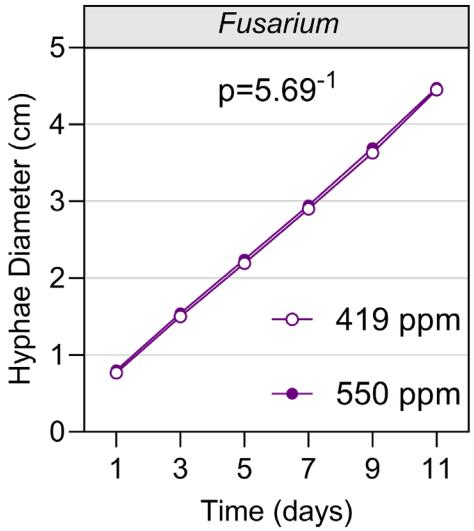

Figure S10. CO_2 concentration does not impact *in vitro* growth of *Fusarium virguliforme*. Hyphae diameter was measured every 2 days over 11 days. Three experiments were conducted simultaneously using 10 plates per experiment, for each CO_2 treatment. Data points represent mean values across three replicates conducted simultaneously in independent CO_2 control chambers. P-value was computed based on an F-test for the interaction effect between CO_2 and time in linear mixed effect model analysis.

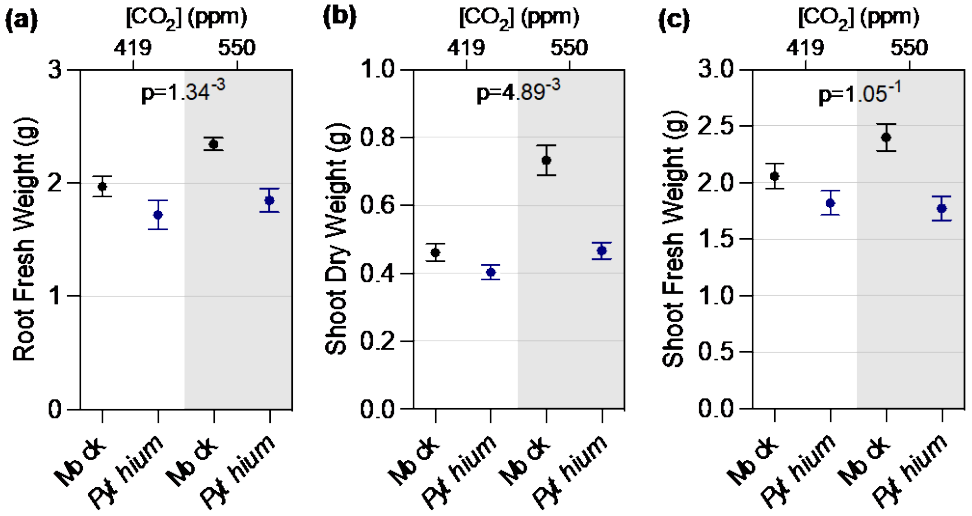

Figure S11. Soybean root and shoot biomass is impacted by eCO_2 in *Pythium sylvaticum* infected plants (a) Root fresh weight, **(b)** shoot dry weight and **(c)** shoot fresh weight in mock or *P. sylvaticum*-infected plants 21 days after inoculation. Experiments were conducted in triplicate using 6 plants per treatment, for each CO_2 condition. Triplicate experiments were conducted simultaneously in independent CO_2 controlled chambers. Data points represent mean values across the three replicates with standard error bars. P-values were computed based on F-tests for the interaction effect between of CO_2 and *Pythium* treatment in linear mixed effect model analysis. Fourth power and log transformation were applied for root fresh weight and shoot dry weight respectively due to unequal variance on the original scale.

1419

1420

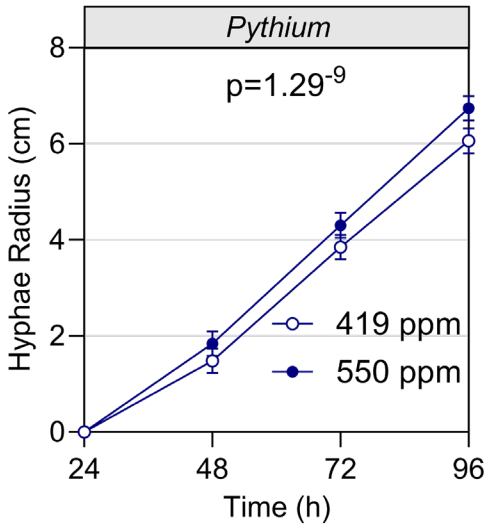

1421

1422

1423 **Figure S12. *In vitro* growth of *Pythium sylvaticum* is accelerated under eCO_2.** Experiments were
1424 conducted using 10 plates per treatment for each CO_2 condition in triplicate. The three experiments were
1425 done simultaneously in independent CO_2 controlled chambers. Hyphae radius was measured every 4 h
1426 over 32 h. Data points and bars represent mean values and standard error across the three replicates.
1427 P-value was computed based on an F-test for the interaction effect between CO_2 and time in linear mixed
1428 effect model analysis.
1429

1430

1431

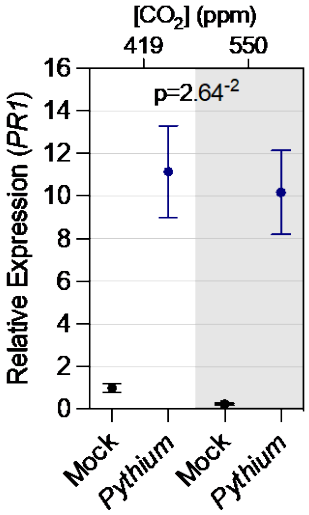

1432

1433

1434 **Figure S13. Expression of the SA marker gene, *PR1*, in roots of plants infected with *Pythium***
1435 ***sylvaticum* in *a*CO_2 and *e*CO_2.** RT-qPCR analysis was conducted using RNA extracted from soybean
1436 roots 14 days after inoculation using gene specific primers for the SA marker gene *PR1* and *Skp1* was
1437 an internal reference control. Experiments were conducted simultaneously in three independent CO_2
1438 controlled chambers using 6 plants per treatment for each CO_2 concentration according to a replicated
1439 complete block design. Data points represent mean values across the three replicates with standard
1440 error. P-value was computed based on an F-test for the interaction effect between CO_2 and *Pythium*
1441 treatment in linear mixed effect model analysis on log-transformed data.